Study of Electrokinetic Response for Drug Susceptibility of Mycobacterium Tuberculosis Complex Cells

Shinnosuke Inoue

A dissertation
submitted in partial fulfillment of the
requirements for the degree of

Doctor of Philosophy

University of Washington
2014

Reading Committee:
Jae-Hyun Chung, Chair
Amy Shen
Kyong-Hoon Lee

Program Authorized to Offer Degree:
Mechanical Engineering

University of Washington

Abstract

Study of Electrokinetic Response for Drug Susceptibility of *Mycobacterium Tuberculosis* Complex Cells

Shinnosuke Inoue

Chair of the Supervisory Committee:
McMinn Endowed Associate Professor Jae-Hyun Chung
Department of Mechanical Engineering

The alarming increase of multi-drug resistant tuberculosis (MDR-TB) has become a serious issue, especially with TB affecting nearly a third of the global population and claiming over a million lives each year. Drug resistance emerges from gene mutations and improper treatment regimens of the drug-susceptible patients, which is transmitted to others when left undetected and untreated. Testing every patient for drug-resistance would be ideal; however, the additional time and resources available for current supplementary tests for drug-resistance are severely limited. The main challenge of drug susceptibility testing is in discovering a simple and inexpensive method.

Drug-susceptibility tests can be differentiated into two categories of phenotypic or genotypic methods. Genotypic methods such as INNO-LiPA Rif, GenoType MTBDR, and Gene Xpert MTB/RIF are very rapid with high sensitivity and specificity, but suffer from the trade-off

of high cost, power supply, and requirement of skilled trained personnel. It is also challenging in that the target drug-resistance sequences should be identified prior to running the tests. Phenotypic drug-susceptibility tests such as MGIT, NRA, and MODS are based on detection of bacterial growth in the presence of antibiotics. Although very reliable and mostly cheap, it requires trained personnel and relatively slow, taking weeks for results. Thus low-cost yet rapid identification of patients with MDR-TB is crucial for increasing chances of survival and controlling the possibility of transmission.

To address the need for a low-cost and direct detection of TB, we developed a sputum sample preparation protocol and a point-of-care TB diagnostic device based on the previous microtip platform. The newly developed sputum protocol was biosafe while retaining the integrity of the antigens so that it can be used in BSL 1 and 2 labs. The biosafe sputum samples were used in the microtip immunofluorescence sensor, where it combines fluid flow circulation and an AC electric field to concentrate target cells in a 1 mL volume to the microtip surface. The surface of the microtip was decorated with IgY antibodies specific to *Mycobacterium* to capture these cells. Once captured, the microtip sensor was labeled and washed for immunofluorescent detection. The device was automated from the beginning of cell capture to the washing of the fluorescent antibodies to minimize operational errors and manual labor. The automated immunofluorescent microtip sensor takes 30 minutes for detection with a detection limit of 100 CFU/mL.

To study electrokinetic effects of viable and non-viable, control and heat-killed Bacillus Calmette-Guérin (BCG) cells were tested on planar electrodes with frequencies ranging from 1 kHz to 10 MHz to determine if the microtip assay will be capable of being implemented as a

drug-susceptibility test. Electrophysiology of cells changes upon cell death, especially when the cell wall and membrane is compromised, changing the electric properties. By analyzing the AC electroosmotic and dielectrophoreic forces, the frequency of 5 MHz was chosen to differentiate viable and non-viable BCG. At the chosen frequency, BCG cells treated with temperatures of 50ºC ~ 80ºC were tested to determine the temperature influence on cell integrity. A transition temperature to differentiate viable and non-viable BCG cells was found to be 60ºC by dielectrophoresis (DEP). Over the transition temperature the lipid cell wall becomes more permeable, which reduces the DEP force the cell experiences. Heat-killed cells treated at 85ºC were shown to be able to be differentiated from control. The cells were further analyzed by characterizing their dielectric properties by matching the experimental crossover frequencies at various medium conductivities. This showed heat-killing decreased the cell envelope capacitance and cytoplasm conductivity, which was shown to be deformed under SEM.

To study drug-effects on DEP, first line TB drugs of rifampin (RIF) and isoniazid (INH) were used to treat BCG cells and compared with untreated BCG cells on planar electrodes. RIF and INH were chosen due to their significance in treatment of TB and their different treatment mechanism. RIF inhibits RNA transcription with no direct interaction with the cell wall whereas the INH inhibits synthesis of mycolic acids in the cell wall structure. Frequency of 5 MHz was employed to differentiate drug-treated and non-treated BCG cells. Cell count of attracted cells showed RIF with similar responses to control, whereas INH-treated cells could be differentiated by the 4^{th} day. RIF-treated cells are only differentiated from control by comparing the aggregation and clusters of cells measuring the fluorescence intensity. The properties of drug-treated cells were also characterized by matching the crossover frequencies at various medium

conductivities. RIF-treated cells showed partial change in the cytoplasm conductivity, while INH-treated cells showed the largest change in the cell envelope capacitance as well as the cytoplasm conductivity. The DEP response correlated with the expected drug mechanism of the administered antibiotic.

The future work will entail evaluation of the microtip and nanotip biosensor as drug-susceptibility tests.

Table of Contents

List of Figures

Page

List of Tables

Page

Acknowledgements

I would like to express my sincere appreciation to my advisor Professor Jae-Hyun Chung for his valuable advice, encouragement and support throughout the years. I may not have pursued my doctorate without his strong belief in my abilities and may not be where I am today. In that same regard, I would like to also thank Dr. Kyong-Hoon Lee for his continuous support and advice.

I would like to thank my committee members Professor Dayong Gao and Professor Amy Shen for their feedback and support. I would also like to thank Dr. Gerard A. Cangelosi for his in-depth discussion on microbiology and fruitful collaboration with him and his group.

Finally, I would like to thank my close colleagues and loving family. Thank you to my dear friends that kept my sanity in check and to stay focused on my graduate work. To my family, who this dissertation is dedicated to, thank you for your everlasting patience and continued love and support throughout these years. I was able to pursue my dreams and complete my graduate studies thanks to them.

This dissertation would not have been possible without the funding from Catalysis Foundation for Health, NSF Career Award (ECCS-0846454), and National Institute of Allergy and Infectious Disease (R01 AI093418).

Chapter 1: Introduction to Drug-susceptibility Tests for Tuberculosis

1.1 Introduction

Tuberculosis (TB) is caused by *Mycobacterium tuberculosis* (MTB) bacteria, affecting nearly a third of the global population and claiming over a million lives each year [1-3]. Those with latent or dormant TB do not show symptoms until it becomes active when their health declines and the immune system can no longer suppress the infection. Thus it is highly problematic for young [4] and old people [5], more so if they are immunocompromised with HIV [6]. Once active, infected people are considered highly infectious and should be treated immediately. A bystander only needs to inhale a few aerosolized germs (via coughing or sneezing) to also become infected [7]. To make matters worse, 95% of TB cases and deaths are concentrated in developing countries. In order to ensure successful treatment, correct choice of antibiotics and its concentration must be administered for a six month period [2, 8]. Failure of proper treatment due to delayed diagnosis, inadequate treatment regimen, or noncompliance by patients may result in multi-drug resistant (MDR) TB strains or extensively drug-resistant (XDR) TB strains [8-10]. MDR TB strains are defined as resistance to one of the first line drugs of isoniazid (INH) or rifampicin (RIF). XDR TB strains are defined as resistance to MDR drugs and second line drugs as well as any fluoroquinolone. The World Health Organization (WHO) estimates that about 440,000 MDR-TB new cases occur every year, with 150,000 resulting in death [8, 10]. The fatality rate is increased for those co-infected with HIV.

There has been a great emphasis on development for point-of-care diagnostic tests; however, tests for drug-susceptible or resistant TB still require laboratory infrastructure. Even so, many countries are inadequate for conventional laboratory testing. Among the 36 countries in the combined list of 22 high-burdened countries and 27 high MDR-TB burden countries, 20 had less than the benchmark of one laboratory capable of performing culture and drug susceptibility testing per 5 million population [8, 10]. In 2010, only a small portion of notified cases were tested for drug susceptibility. Globally, less than 2% of new cases and 6% of retreatment cases were tested for MDR-TB [8, 11]. These factors may have contributed to the alarming rates of MDR-TB and emergence of XDR TB. By March 2010, 58 countries have reported accounts of XDR-TB to WHO [10]. Therefore, assessing the bacteria's susceptibility to drugs is as crucial as development of rapid diagnosis and treatment to cure TB. The Global Plan to cure the world of TB set by WHO includes targets that by 2015, all new cases of TB considered high risk of MDR-TB and 100% of retreatment cases should be tested for drug susceptibility. To reach the Global Plan's goal by 2015, it is imperative to develop a point-of-care method and diagnostic device to rapidly detect TB for resistances, especially for RIF and INH.

To understand the shortcoming of current drug susceptibility tests, this chapter will review the primary diagnostic tool for TB, and the two categories of drug susceptibility tests of phenotypic and genotypic methods.

1.2 Smear Microscopy

In low and middle-income countries, direct sputum smear microscopy is the primary diagnostic method used to diagnose pulmonary TB [12-14] in spite of modern advancements. It is used to identify sputum smear-positive samples which are the most infectious cases. Most common method used is with Ziehl-Neelson staining, where carbol-fuchsin dye initially stains the organisms red. The sample is then decolorized using acidic ethanol and counterstained with methylene blue for contrast. The high lipid content of the mycobacterial cell wall helps retain the red dye from being removed unlike other bacteria. Smear microscopy is very inexpensive, fast, and specific for *M. tuberculosis* in high incidence areas [14, 15], all traits wanted for low-resource diagnostic methods.

Unfortunately, smear microscopy has poor sensitivity, ranging from 20-80%, and has limited value for those coinfected with HIV [16]. Many have attempted to improve the accuracy and efficiency of microscopy with thoughts such as light-emitting diode fluorescence detection [14], same-day sputum collection [17], and bleach processing [18, 19], but came to the conclusion that there is insufficient evidence that these methods will outweigh the current benefits of microscopy [16]. The last disadvantage is smear microscopy gives very little information when it comes to drug-susceptibility. One of the few times it does provide insight on drug susceptibility is when a patient undergoing anti-TB treatment after 5-months is found with smear-positive sputum [20]. At this stage of treatment, the patient should be smear-negative or culture-negative as long as they followed the regimen and given proper treatment. If they are not, they are considered to have failed the treatment and are evaluated for drug resistant TB. What is worse is that patients that receive treatment for 2 months can be smear-negative even if they have MDR-TB. In one study, 75% of patients known to have MDR-TB were smear-negative after 2

months of treatment and would therefore be missed and released back into society had they have not known and solely relied on smear microscopy [21]. Thus the primary diagnostic method of smear microscopy currently used in low-resource settings is not sufficient to diagnose and control TB, especially MDR-TB.

1.3 Phenotypic Drug-Susceptibility Test

Culture-based diagnosis remains to be the most sensitive assay in testing for TB and very reliable. Even with development of molecular assays, culture may be used to reconfirm the results. Although relatively slow, solid media such as Löwenstein-Jensen or liquid media such as Kirchner and various Middlebrook formulations (7H9, 7H10, 7H11) have been used for years. Time till detection of growth of mycobacterial species was significantly shortened using semi- to fully automated radiometric liquid culture systems [22]. However, due to problems with staff labor and disposal of radioisotopes, new automated liquid media systems (ALMS) that relied on non-radiometric detection of growth were developed. These techniques such as BACTEC 9000 (Becton Dickinson), Mycobacterial Growth Indicator Tube (MGIT; Becton Dickinson), and MB/BacT (Biomerieux) have been compared and studied by many groups [23-25]. By measuring the changes in gas pressure, carbon dioxide production, or oxygen consumption fluorimetrically or colorimetrically, smear-positive sputum samples became detectable typically after 14 days and most mycobacteria within 21 days [26].

Conventional drug susceptibility test (DST) methods are based on culture and detection of bacterial growth in the presence of antibiotics. Although sensitive, DST for slow growing cells such as mycobacteria results from culture is very slow and can take 6-12 weeks [27]. Additionally, all culture-based tests with culture manipulation require a BSL 3 laboratory and extensive personnel training. ALMS, such as MGIT system, have reduced the total turnaround time to 3-4 weeks and are fully automated with continuous monitoring. Well-funded clinical laboratories can detect TB cases in 7 to 14 days with BACTEC and MGIT [28]. The main drawbacks of ALMS is there need for an uninterrupted supply of commercially manufactured consumables and have higher associated costs compared to solid media [29].

Several less expensive, noncommercial culture and drug-susceptibility testing have been developed and evaluated to try to alleviate this problem. Of these, microscopic observation drug susceptibility assay (MODS) [30], nitrate reductase assay (NRA) [31], and colorimetric redox indicator (CRI) has shown evidence it can detect MTB as well as resistances to INH and RIF and has been endorsed by WHO [29]. These assays require inexpensive, generic laboratory materials unlike ALMS. Sensitivity and specificity ranged from 95-98% and 96-100% for MODS and 95-98% and 99-100% for NRA, respectively [29, 32]. A costing evaluation showed NRA and MODS are the most cost-efficient method for large number of patients [27, 33] and thus may be an alternative to commercially available ALMS drug-susceptibility tests in resource restricted locations. The time for detection, however, is not necessarily faster and the testing capability of drugs is limited. The endorsed methods may serve as an interim solution for resource-limited areas but conventional culture and drug-susceptibility tests are still required in all settings [29].

1.4 Genotypic Drug-Susceptibility Test

Genotypic methods are generally nucleic acid amplification tests (NAATs) and are molecular diagnostic approaches which are used for detection of specific species of TB (such as MTB), differentiating from non-tuberculous mycobacteria, and identifying drug resistance. NAATs can be separated into main categories of DNA sequencing, solid phase hybridization assay, and real-time polymerase chain reaction (RT-PCR).

1.4.1 DNA sequencing

DNA sequencing is the process of identifying the precise sequence of the nucleotides in the DNA molecule. It is very reliable for detection of species of TB and in some cases drug resistances such as RIF, where detection of the short mutation in *rpoB* is a strong indicator of resistance; however, sequencing is not as useful when the mutations are scattered in a large segment of the gene, silent mutations which does not have any significant phenotypic change arise, or when many different genes make up the resistance [34, 35]. This is the case for INH, where at least four genes are known to be involved with the resistance [36, 37]. Sequencing can be expensive, requires high level of technical competence, and may use radioactive labeling which needs to be properly disposed of, making it unsuitable for high burden laboratories.

1.4.2 Solid phase hybridization

Solid phase hybridization assay detects mutations by observing if probes immobilized on solid surfaces hybridize with an amplified gene sequences. Hybridization is determined when enzymatic color reaction or fluorescence signal is observed. Failure of signal indicates mutations in the sequence, and the mutation itself can be determined if a complementary mutation sequence probe is observed with fluorescence.

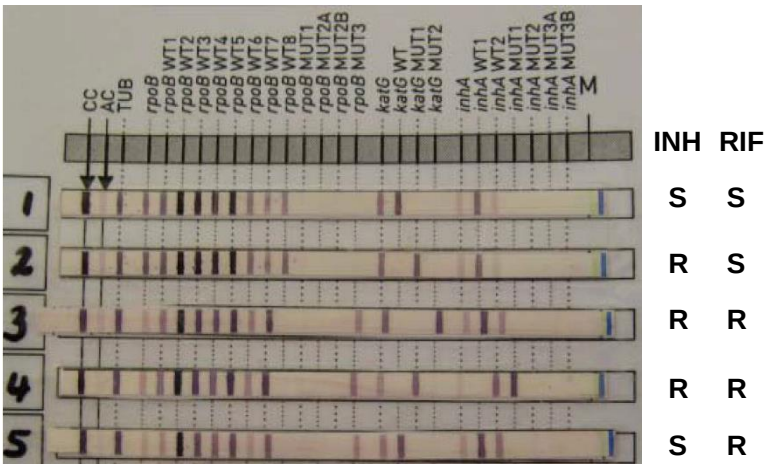

Figure 1.1. Example results of GenoType MTBDR*plus*. The strips show different readings for INH and RIF susceptibility (S) or resistance (R) or both. (M.Barnard et al, AJRCCM 2008)

The most common type of solid phase hybridization assay is line probe assays (LPAs), where probes are attached to nitrocellulose strips. Two commercially available test endorsed by WHO are GenoType MTBDR and MTBDR*plus* (Hain Lifescience, Nehren, Germany) [38] and INNO-LiPA Rif.TB (LiPA; Inogenetics, Ghent, Belgium) [39, 40]. These methods can simultaneously detect *M. tuberculosis* complex and specific mutations in the *rpoB* gene for resistance to RIF. GenoType MTBDR*plus* can also simultaneously detect for *katG* and *inhA* gene for INH resistance. In a systematic review and meta-analysis, 12 out of 14 isolates evaluated with LiPA had sensitivity greater than 95% and specificity of 100% [41]. In a different systematic meta-analysis, the pooled sensitivity and specificity for GenoType MTBDR was 99% and 98%, and for GenoType MTBDR*plus* was 99% and 99%, respectively [32]. These LPAs are simple to perform but require expertise in molecular biology and PCR techniques. They also have lower sensitivity and specificity in smear-negative samples and have a slower turnaround time of 1-2 days compared to other genotypic methods.

1.4.3 Real-time PCR

RT-PCR allows for quantitative monitoring of DNA amplification while they occur. Fluorescence signal measured by the assay is proportional to the amplified sequences. Different types of probes have been used, such as fluorescent resonance energy transfer (FRET) [42], molecular beacons [43], and bioprobes [44]. The assay can also detect heteroresistance by discriminating different subpopulations in clinical samples, thus allows for early detection of emerging resistances [34]. The biggest advantage of RT-PCR is the time and lower risk of contamination. Results can be provided in 1.5 – 2 hours after DNA extraction, thus in a single office or clinic visit. The samples are kept in closed tubes during detection so they are safe to handle and less likely to have cross contamination. The downside is the expensive equipment and reagent cost, as well as a need for skilled technicians.

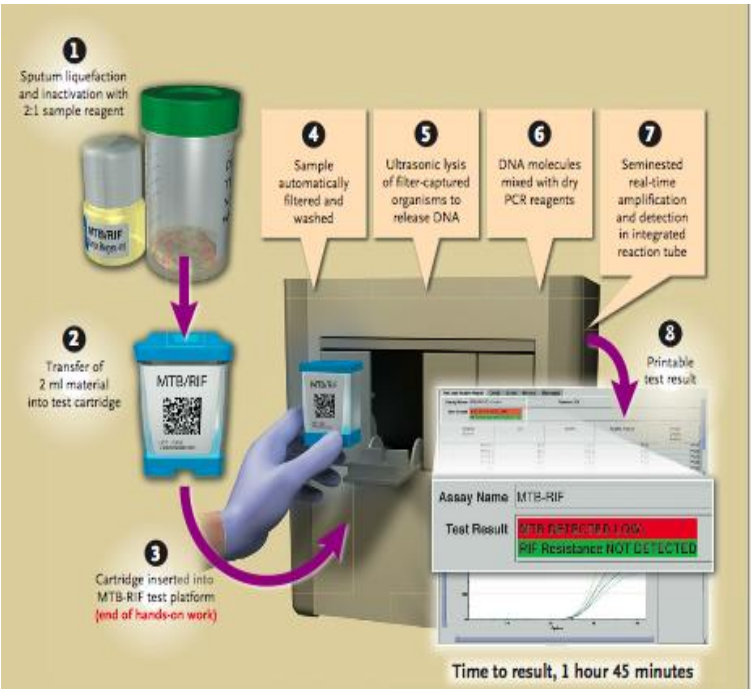

Figure 1.2. RT-PCR machine of GeneXpert.

WHO has endorsed Xpert MTB/RIF (Sunyvale, CA) [8], a single-use sample-processing cartridge PCR system capable of results in 2 hrs. The system has integrated sample decontamination, hands-free operation, on-board sample processing, and ultra-sensitive hemi-nested PCR. The simple and robust assay needs minimal training and less than 5 min of hands-on time [45-48]. Clinical samples found sensitivity of 98-100%, 72% for smear-negative samples, and specificity of 100% [45]. An evaluation by WHO also found similar results with 98% of sensitivity and 98% of specificity in detecting TB and RIF resistance [8]. The assay is robust enough to be implemented in decentralized levels of health system and available for preferential pricing for low and middle-income countries. Despite these advantages, however, the system does have its drawbacks. The device is not portable and restricted to the laboratory or clinic, requiring continuous electrical power supply, security, and maintenance. Even with the discount, the anticipated cost of the system ($17,000 US, excluding tax and delivery charges) and individual test cassettes ($16 US) is likely to limit the implementation of this test [49]. In 2011, only 26 of 145 countries eligible to purchase the system and sample cartridges at discounted prices had done so [2]. Therefore, rapid molecular methods cannot completely replace conventional DSTs, but can serve as a rapid supplement [50].

1.5 Summary

Conducting DSTs for all new patients with TB has been considered impractical and expensive; however, with the rise of MDR-TB as well as XDR-TB, it is important to have early detection and treatment to better manage this global epidemic. There is a need for rapid yet inexpensive method to detect drug-susceptibility. Table 1 summarizes the significant drug susceptibility methods mentioned in this section.

Table 1.1. Summary of drug-susceptibility testing methods

Method	Detectable resistance	Time till detection	Cost per test	Pros	Cons	Reference
Phenotypic methods						
Mycobacterial growth indicator tube (MGIT)	Any	7-14 days	$32 - $56	• Fully automated • Rapid results • Ride range of drug resistance test	• High contamination rate • Cost • Uninterrupted supply of commercial consumables	[28]
Nitrate reductase assay (NRA)	Rifampin and Isoniazid	7-28 days	$3 - $4	• Standardized method • Minimal equipment and readily available consumables • Non-commercial – low cost	• Moderate indeterminate rate • Limited drug range • Exposure risk to technicians	[32, 33]
Microscopic observation drug susceptibility (MODS)	Rifampin and Isoniazid	4 - 21 days	$1.40 - $3.50	• Standardized method • Minimal equipment and readily available consumables • Non-commercial – low cost	• Requires inverted light microscope • Limited drug range • Exposure risk to technicians	[32, 33]
Genotypic Methods						
INNO-LiPA RIF (LiPA)	Rifampin	6 - 48 hrs	$30 - $116	• Automated and rapid • Highly sensitive and specific for culture isolates	• Requires expertise in molecular biology • High cost • Does not test for INH • Low sensitivity and specificity in smear-negative	[39-41]
GenoType MTBDR and MTBDRplus	Rifampin and Isoniazid	6 - 48 hrs	$35 - $65	• Rapid and relatively simple • Highly sensitive and specific • Test for both RIF and INH	• Requires expertise in molecular biology • High cost • Lower sensitivity for INH • Low sensitivity and specificity in smear-negative	[32, 38]
Xpert MTB/RIF	Rifampin	1.5 - 2 hrs	$15 - $120	• Commercial and automated • Closed system with minimal biosafety • Very rapid • Highly sensitive and specific	• Requires stable electrical power • Does not test for INH • High cost	[11, 45]

1.6 Objectives

The main objective of this dissertation is to study the electrokinetic responses of *Mycobacterium tuberculosis* complex cells after exposure to first-line antibiotic drugs of rifampin and isoniazid so that it may be used for rapid detection of drug susceptibility. First, a rapid and occupationally safe diagnostic device is developed to detect *Mycobacterium* directly from processed sputum. The device shows low limit of detection but has not been evaluated for differentiating viable and non-viable (heat-killed or drug-killed) cells. A fundamental study on the combination of electrokinetic forces of dielectrophoresis and AC electroosmosis is investigated using a single planar electrode system. The system is then utilized to study dielectrophoretic and electroosmotic flow of cells in different electrophysicological states. This is used to determine the electrical properties as well as experimental parameters needed to differentiate the viable and non-viable cells. By determining the optimal experimental conditions, the new diagnotis device should be capable of drug-susceptibility tests.

Chapter 2: Development of Biosafe Microtip Immunosensor for Rapid TB Diagnosis

2.1 Introduction

A challenge for point-of-care diagnosis of TB is developing an inexpensive yet rapid assay capable of detection from sputum for low-resource, BSL1 or BSL2 settings. Rapid diagnosis is important not only for patient care but also for prevention of disease transmission. TB infections commonly occur through aerosol transmission in communities [51] but occupational infection of healthcare workers and laboratory personnel can occur through multiple routes. Due to their exposures, these workers are at increased risk of both TB infection and disease [52, 53]. There has been a lot of development in microfluidic and electrokinetic approaches [54-57] for rapidly detecting bacteria and biomolecules in samples, however, the methods have not been applied to viscous sputum samples.

The standard protocols for detecting *M. tuberculosis* in sputum samples are smear microscopy and bacterial culture. Sputum smear microscopy is the major diagnostic tool used in many resource-limited settings [26, 58]. The method lacks sensitivity but is relatively rapid, simple, and inexpensive in areas with high prevalence of TB [14]. Bacterial culture is more sensitive than microscopy but may take several weeks to yield results [59]. Laboratory infrastructure is needed for either microscopy or culture, and the latter requires BSL3 containment to minimize the risk of occupational exposure to the pathogen.

With the introduction of the GeneXpert (Cepheid, Sunnyvale, CA, USA), rapid nucleic acid amplification tests are becoming more common in clinical laboratories. The automated, cartridge-based polymerase chain reaction (PCR) assay can be operated outside of BSL3 labs and can diagnose smear-positive TB in two hours with 98% reliability [48]. Although far more rapid than culture-based methods, a two-hour time to result may be too long for some patient visits. For example, an implementation study reported revisions to procedures and interventions to address the problem of patients leaving the clinic or becoming untraceable within the clinic prior to completion of the 2-hour GeneXpert protocol [60]. Moreover, the GeneXpert instrument is expensive to install and operate [49, 58]. Thus, there still remains a need for an inexpensive and rapid assay to detect TB. Newer technologies have enabled the rapid detection of pathogen antigens (either whole-cell or molecular) without requiring nucleic acid amplification and with sensitivity approaching that of PCR [61, 62]. For example, we have previously reported a microtip immunofluorescence sensor capable of detecting 200 CFU/mL of *M. tuberculosis* complex cells in spiked sputum [63]. Using microscale tips, *Mycobacterium* cells were concentrated and captured out of sputum by electrohydrodynamic effects. . The captured cells were detected by low-magnification (20X objective) fluorescence microscopy. Specificity was conferred by a polyclonal antibody that was immobilized on the microtip surfaces. The entire process required 25 minutes to complete, significantly faster than any approved molecular diagnostic method for TB. The device, however, required manual labor where detection relied on skilled technicians and the processed sputum was not occupationally safe (biosafe).

A limitation of antigen detection is the requirement for relatively gentle sample handling. Antigen structure must be at preserved to enable detection by antibodies or other molecular probes. This requirement can be problematic when working with infectious samples such as

sputum from TB patients. For example, sputum samples in our previous test were treated with N-Acetyl-L-Cysteine (NALC) and sodium dodecyl sulfate (SDS) [63]. This process liquefied the viscous sputum samples while preserving antigen integrity, however it did not disinfect the samples. As a result, BSL2 or BSL3 laboratory infrastructure would be required for safe operation when applied to samples from TB patients. Similar limitations are likely to apply to other antigen detection platforms.

In this chapter, we addressed the challenge of inactivating *Mycobacterium* cells and other pathogenic organisms in sputum, while maintaining mycobacterial cell integrity for concentration and immunodetection using the microtip assay. *Mycobacterium* cells are robust and difficult to inactivate without harming antigenic structures. In addition, residual microbicides could "poison" antigen-antibody interactions. To address this challenge, we investigated a synergistic approach, in which moderate heating was used to transiently increase the susceptibility of *Mycobacterium* cells to moderate disinfectant treatment. This strategy was based in part on reports that the waxy, impermeable mycobacterial cell envelope undergoes a reversible phase shift at around 60°C, resulting in a semi-fluid structure [64]. We hypothesized that the altered structure would render the cells more susceptible to damage by mild chemical challenges such as NaOH and detergents. A process was thereby developed that enables the safe molecular detection of *Mycobacterium* cells in settings that lack BSL3 or even BSL2 containment.

This chapter also describes improvements to our microtip platform that renders the process more user-friendly. The improved device is semi-automated to reduce labor and to improve the reproducibility of washing and immunofluorescence detection. To characterize the performance of the improved device and protocols, the device was tested for detection of *M. tuberculosis* complex (strains H37Ra and BCG Russia), non-tuberculous *Mycobacterium* (NTM)

species (*M. avium* strain 104 [65] *and M. smegmatis* mc^2155), and *Staphylococcus epidermidis* spiked into sputum samples. To render the assay more affordable, a low-cost, battery operated fluorescence microscopy system was validated as a replacement to previously-used high-resolution system.

The sputum processing protocol was developed with the help of Annie Becker and Zhiquan Shu. The design of the automated device was made by Dr. Kieseok Oh at Nanofacture, Inc. The automated microtip sensor was evaluated with the treated sputum in the collaboration with Jong-Hoon Kim and Morgan Hiraiwa.

2.2 Materials and Methods

2.2.1 Biosafe sputum liquefaction protocol

Human sputum was purchased from Bioreclamation, LLC (Westbury, NY) and stored in 300 µL aliquots in cryogenic tubes at –80°C until use. Prior to running experiments, frozen samples were thawed at room temperature and spiked with cultured bacteria where indicated. To run the biosafe protocol, 600 µL of spiked sputum (300 µL of sputum with 300 µL of bacterial cell suspension suspended in PBS) was supplemented with 300 µL NaOH solution (0.4M), 300 µL sodium dodecyl sulfate solution (4% SDS), and 15 glass beads with diameter of 3 mm. The suspension was vortexed briefly. Tubes were incubated in a 60°C water bath for 10 minutes, then vortexed at 1400 rpm for 5 minutes. Subsequently, 1 mL out of the 1.2 mL suspension from each tube was transferred to an empty tube and 250 µL HEPES buffer (1M) was added to each tube to neutralize the NaOH. The current and previous sputum processing protocol is shown in Figure 2.1.

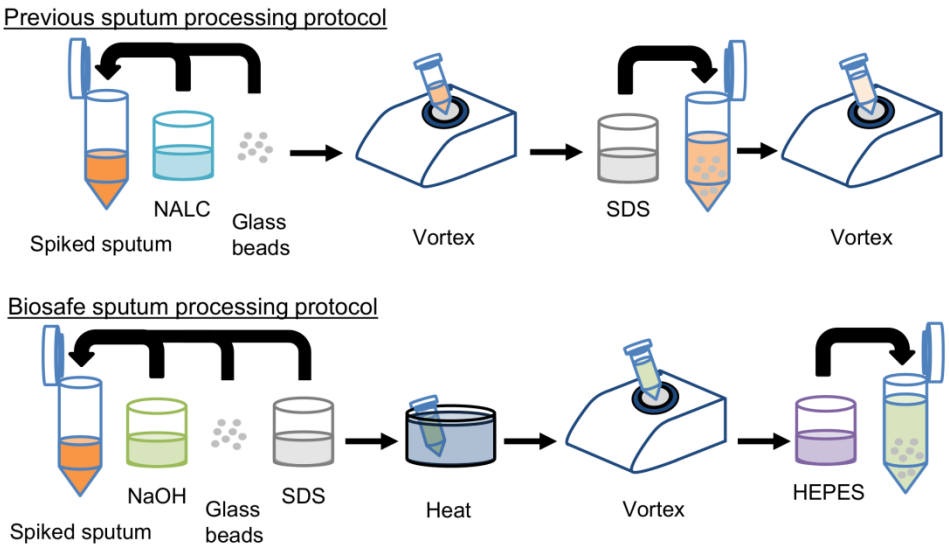

Figure 2.1. Comparison of the previous protocol (top) and biosafe sputum processing protocol (bottom).

2.2.2 Bacterial culture

All organisms used in this study were cultivated in a shaker at 37°C. *Mycobacterium* strains were cultured in Difco Middlebrook 7H9 Broth (BD Diagnostics, Sparks, MD) supplemented with 10% (v/v) ADC enrichment and 0.05% Tween 20. All other organisms were grown in trypticase soy broth.

2.2.3 Microbiological analysis of biosafe protocol-treated samples

Cultured *M. tuberculosis* complex cells were suspended either in phosphate buffered saline (PBS) or in human sputum samples as described above, at estimated densities of approximately 1 x 10^7 CFU/mL [based on optical density (A_{600}) measurement of cultures]. After the various treatments described in this report, 0.1 mL samples of the suspensions were plated in triplicate onto Difco Middlebrook 7H10 agar with 10% (v/v) OADC enrichment (BD Diagnostics, Sparks, MD). Plates were incubated at 37°C for up to 35 days. Untreated sputum

samples rapidly overgrew plates due to the natural flora of sputum by the 21st day. Therefore, no-treatment controls consisted of untreated suspensions of *M. tuberculosis* complex cells in PBS. This strategy enabled us to quantify viable *M. tuberculosis* complex cells in untreated controls.

2.2.4 Microtip assay

The semi-automated, immunofluorescence microtip assay, a new design based from our previous device [63], is shown in Figure 2.2. The microtip immunosensor device is designed for rapid identification of MTB in sputum samples. The sensor is a microtip with immobilized polyclonal IgY antibodies on its surface. The antibodies were raised against whole acetone-treated *M. tuberculosis* complex cells. On the surface of the device is a disposable aluminum well to hold the treated sputum. In addition, PDMS wells to hold rinsing solutions of deionized water (DI water) and SDS solutions (1% in DI water) as well as a fluorescent antibody solution for labeling. The labeling antibody is the same polyclonal IgY as the antibody on the sensor. Housed under the wells is a vibration motor used to circulate sample during the capture process, and two linear motors to precisely control the position of the microtip sensor.

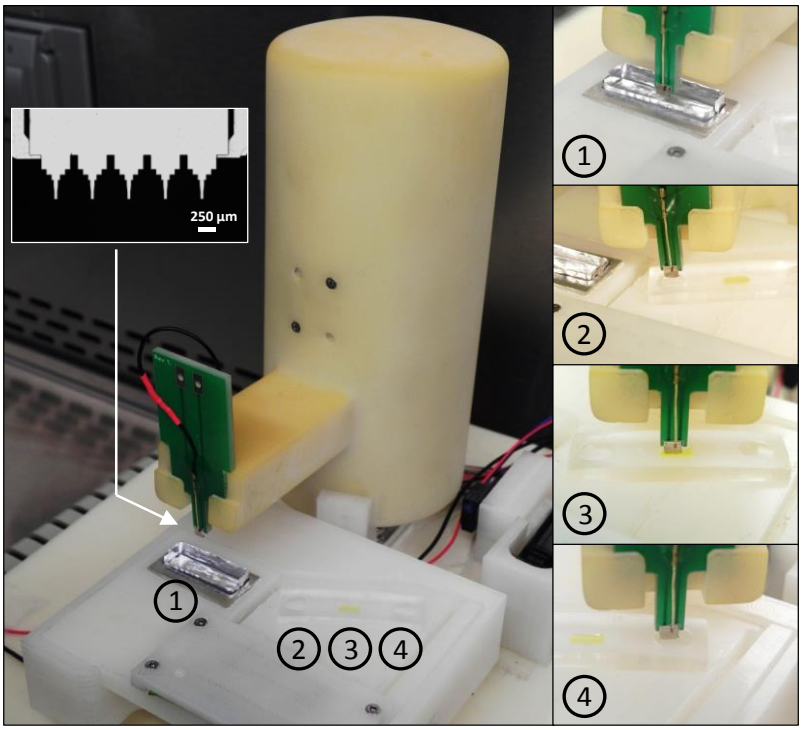

Figure 2.2. Semi-automated microtip system for concentration and detection of *M. tuberculosis*. The microtip used in the device is shown with scale bar of 250 µm. Components are as follows: (1) Sample well in which cells are concentrated and captured onto the microtip, (2) initial rinsing well with 1% SDS solution, (3) labeling well in which cells captured on microtip are bound to fluorescent antibody, (4) final rinsing well with DI water.

The operation begins with the functionalized microtip being immersed into the aluminum sample well containing 1 ml of treated sputum (Fig. 2.2-1). Cells are rapidly concentrated to the microtip by a circulating flow produced from mechanical vibration, working in concert with electrokinetics force of dielectrophoresis (reviewed in Chapter 3) from an applied AC field (Fig. 2.3). The vibration motor under the aluminum well generates a convective flow to bring cells spaced throughout the volume of the solution toward the microtip. Cells near the vicinity of the microtip are polarized by a function generator (Agilent 33220A, Santa Clara, CA) which applies

an AC electric field of 5 MHZ and 20 $V_{p.p.}$ for 2 minutes, creating a force known as dielectrophoresis to attract the cells to the edges of the microtip. Large, non-specific cells are removed when the microtip functionalized with antibodies is withdrawn from the solution. During withdrawal, capillary force pulls the larger particles off the tip-end [66-68]. The microtip with captured cells is quickly rinsed in SDS solution (0.1% in DI water) to remove non-specific cells that are not bound to immobilized antibodies (Fig. 2.2-2). The tip is then translocated to the fluorescent antibody solution (10 µl, 2 mg/ml) where bound cells are labeled (Fig. 2.2-3). The microtip is lastly rinsed in DI water (160 µL) to remove unbound fluorescent antibodies (Fig. 2.2-4). The fluorescence images of microtips are captured by low-power fluorescence microscopy (Olympus BX-41, Olympus America Inc., Melville, NY). Fluorescent intensity is digitally measured and analyzed to yield a numeric result.

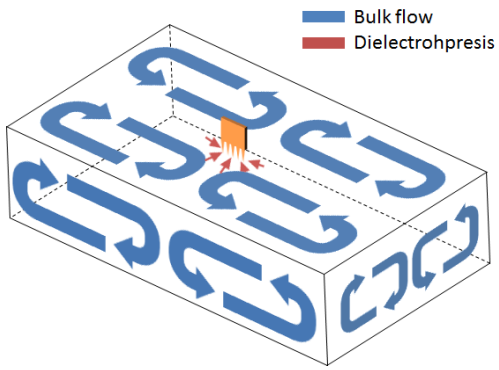

Figure 2.3. Rapid concentration mechanism using a combination of bulk fluid flow with dielectrophoresis.

In an indication of the reproducibility of these methods, the experiments reported here were conducted over a period of 4 months and fresh bacterial cell cultures were used each week. Fresh batches of functionalization reagents and microtips were used each month. Sputum samples were purchased in several batches. In addition, three different research personnel

operated the semi-automated microtip assay with comparable results. In this fashion, variability related to sample composition, target cell physiology, and human errors were evaluated.

2.3 Results

2.3.1 Inactivation of *M. tuberculosis* in sputum

Experiments were performed to evaluate the effects of the new protocol on the viability of *M. tuberculosis* complex cells. Initial experiments were conducted on *M. bovis* BCG cells suspended in PBS. Suspensions were exposed to varying temperatures (room temperature to 80°C), for varying periods of time (2 to 15 minutes), and with varying concentrations of NaOH (0 to 1 M). At room temperature, protocols utilizing NaOH at concentrations up to 1 M did not significantly reduce the viability of BCG in PBS. When cells were treated with elevated temperatures (50°C, 55°C, and 60°C) in PBS in the absence of chemical challenges, only partial loss of viability was observed (lawns of colonies on plates were visibly thinned but still too numerous to count). In contrast, the complete biosafe protocol, which involved treatment with 0.1 M NaOH and 1% SDS (final concentrations) at 60°C for ≥5 minutes, reduced the viability of BCG approximately 10^6-fold (Table 2.1). Shorter incubation times (2 min) or lower temperatures (room temperature or 50°C) were less effective. In two additional experiments, 5 to 10 min of treatment at 60°C with 0.1 M NaOH and 1% SDS always resulted in $\geq 10^6$-fold loss of viability of BCG. To maximize occupational safety a 10-min protocol was used in subsequent experiments.

To test the protocol's effect on microorganisms present in unspiked sputum, we plated both untreated and treated sputum on Middlebrook 7H10 media. The untreated plates were found to be overgrown with a variety of both bacteria and fungi, and the biosafe protocol inactivated all culturable (on Middlebrook medium) microorganisms present in the sputum samples.

Table 2.1. Effects of temperature and treatment time on inactivation of BCG cells in PBS.

Treatment time	Colony forming units (CFU)[1]		
	Room temperature	**50°C**	**60°C**
0 min (untreated)	TNTC[2]	-	-
2 min	TNTC	TNTC	234
5 min	TNTC	TNTC	3
10min	TNTC	TNTC	3
15min	TNTC	TNTC	1

[1]BCG cells were suspended in PBS at concentrations of approximately 1 X 10^7 CFU/mL. After treatment of 0.1 M NaOH and 1% SDS, 0.1 mL aliquots were plated on triplicate Middlebrook 7H10 plates with OADC enrichment. Numbers shown are total counts for the three plates after 35 days of incubation at 37C.
[2]TNTC, too numerous to count.

Subsequent experiments were conducted on cultured cells of *M. tuberculosis* strains H37Ra and H37Rv spiked into human sputum. The complete 10-min biosafe protocol inactivated both *M. tuberculosis* strains in sputum by $\geq 10^6$-fold. Table 2.2 shows the results of six experiments conducted on separate sputum samples spiked with *M. tuberculosis* H37Rv. Samples were subjected to the 10-min biosafe protocol with and without bead beating. The protocol consistently resulted in $\geq 10^6$-fold inactivation of H37Rv regardless of bead beating. Although bead beating was found not to be required for pathogen inactivation, we believed it made micotip enrichment consistent by reducing the sputum viscosity. Subsequent experiments used the complete protocol with bead beating.

Table 2.2. Inactivation of M. tuberculosis H37Rv in sputum by using the biosafe protocol.

Treatment	Colony forming units (CFU)[1]					
	Sample 1	**Sample 2**	**Sample 3**	**Sample 4**	**Sample 5**	**Sample 6**
No treatment[2]	TNTC[3]	TNTC	TNTC	TNTC	TNTC	TNTC
Complete protocol	0	0	0	0	0	0
Without bead beating	0	0	0	0	0	0

[1]H37Rv cells were suspended in sputum samples at concentrations of approximately 1 X 10^7 CFU/mL. After treatment, 0.1 mL aliquots were plated on triplicate Middlebrook 7H9 plates with ADC supplement. Numbers shown are total counts for the three plates after 33 days of incubation at 37ºC.
[2]Because untreated sputum samples rapidly overgrew plates due to the natural flora of sputum, no-treatment controls consisted of *M. tuberculosis* cells suspended in PBS.
[3]TNTC, too numerous to count.

2.3.2 Microtip assay

The previous microtip device [63] was remodeled to automate the steps from pathogen cell capture to fluorescence measurement. The modifications described in Methods reduced manual labor and the potential for operator errors. The semi-automated device was evaluated in combination with the biosafe sample processing protocol. The current study also extended previous evaluations by assessing the specificity of the polyclonal antibody for *Mycobacterium* species other than *M. tuberculosis* complex.

The investigation tested a total of 95 separate samples in spiked sputum, including 22 control samples spiked with PBS, 9 with *S. epidermidis* (10^4 CFU/mL), 6 with *M. smegmatis* (10^4 CFU/mL), 10 with *M. avium* (10^4 CFU/mL), and 6 samples for each of four concentrations of BCG and *M. tuberculosis* H37Ra ranging from 10^2 to 10^5 CFU/mL. Bacterial densities were estimated by 10-fold dilutions from 10^7 CFU/mL. After spiking into sputum, the samples were processed by the biosafe protocol. After microtip analysis of the processed samples, fluorescent intensity values were normalized by the equation [Normalized intensity = (fluorescence

intensity-19.2)/19.2]. The value of 19.2 was the average intensity of negative control assays + standard deviation. The error bars represent 95% CI.

Sputum spiked with *Mycobacterium* and processed by the biosafe protocol generated consistently positive signals (Fig. 2.4). A *t*-test with 95% CI was used for significance. Signals generated with *M. avium*, *M. smegmatis*, H37Ra, and BCG differed significantly from negative (non-spiked) control samples (p = 0.004, 0.01, <0.001, and 0.005, respectively). Samples spiked with *S. epidermidis* were statistically indistinguishable from negative controls.

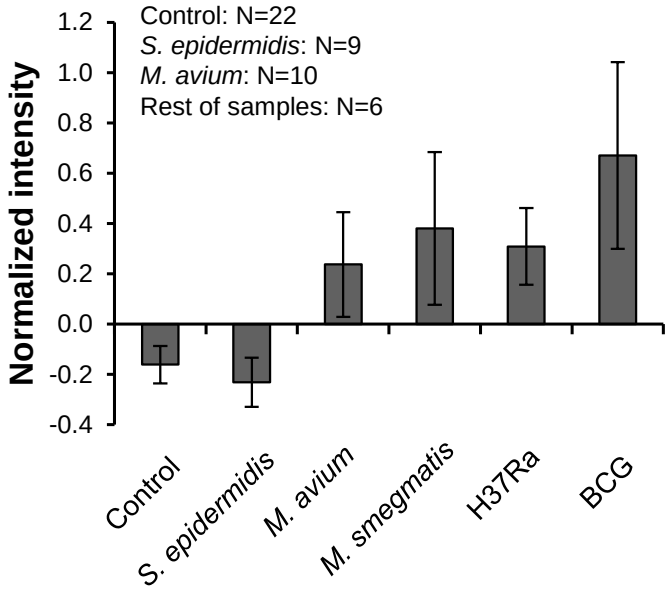

Figure 2.4. Normalized fluorescence intensity results from the microtip assay. Showing the comparison of different species of *Mycobacterium* and *S. epidermidis* at 10^4 CFU/mL.

S. epidermidis was chosen as a specificity control because of its common occurrence in all types of human tissue samples. In addition, the sputum itself was likely to have contained numerous human and microbial cells. Therefore, the specificity of the assay for *Mycobacterium* cells, when conducted on biosafe-treated samples, was evident. However, the assay cross-reacted with the NTM species *M. avium* and *M. smegmatis.* This cross-reactivity was likely to be a

feature of the polyclonal antibody, not a result of the biosafe protocol, because untreated NTM cells were also observed to cross-react with this antibody (data not shown).

The limit of detection of the semi-automated microtip immunofluorescence assay, when conducted on biosafe-treated samples, was determined by testing estimated concentrations of BCG and MTB H37Ra ranging from 10^2 to 10^5 CFU/mL (Fig. 2.5A, B). BCG at or above 10^2 CFU/mL differed significantly from negative controls ($p \leq 0.004$ at all concentrations). The same was observed for H37Ra at or above 10^2 CFU/mL ($p \leq 0.003$ at all concentrations). Thus, the detection limit achieved for both BCG and H37Ra was 100 CFU/mL, similar to the limit reported for samples treated by the previous NALC-SDS method (200 CFU/mL) [63]. As in the previous report, the dose-response curve saturated at low cell concentrations and was not strongly linear. Raw images of microtips after capturing serial dilutions of BCG concentrations are shown in Figure 2.6.

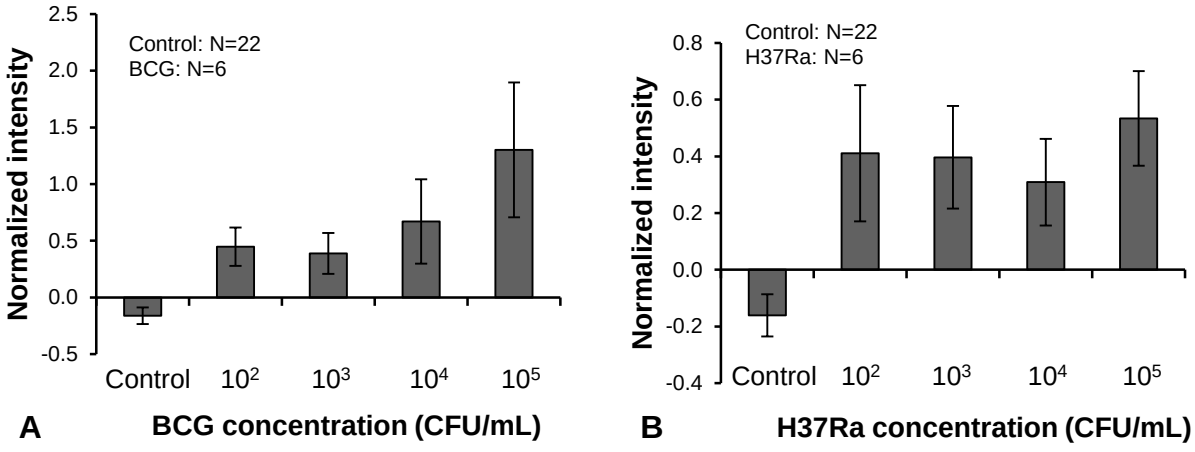

Figure 2.5. Normalized fluorescence intensity results from the microtip assay. (A) Dose response from BCG concentrations ranging from 10^2 to 10^5 CFU/mL. (B) Dose response from H37Ra concentrations ranging from 10^2 to 10^5 CFU/mL.

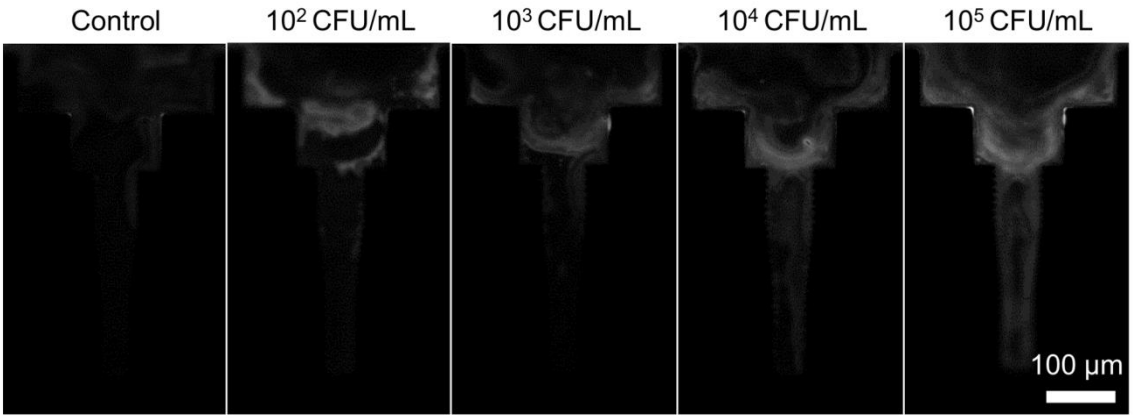

Figure 2.6. Raw fluorescent images (20X objective) of microtips after capture from spiked sputum samples with BCG at densities ranging from 0 (control) to 10^5 CFU/mL.

2.3.3 Compatibility with low-cost fluorescence microscopy.

In order to assess the compatibility of the microtip method with low-cost portable fluorescent microscopes, 8 sputum samples were assayed using the LED-based, battery-powered Lumin™ microscope (LW Scientific, Lawrenceville, GA, USA), along with the more expensive Olympus BX-41. Among the 8 samples, 3 were negative controls and the other 5 were spiked with BCG (10^4 CFU/mL). The Lumin instrument yielded intensity values that were slightly lower than those of the Olympus, however both microscopes distinguished spiked from control samples with similar efficiency (Fig. 2.7).

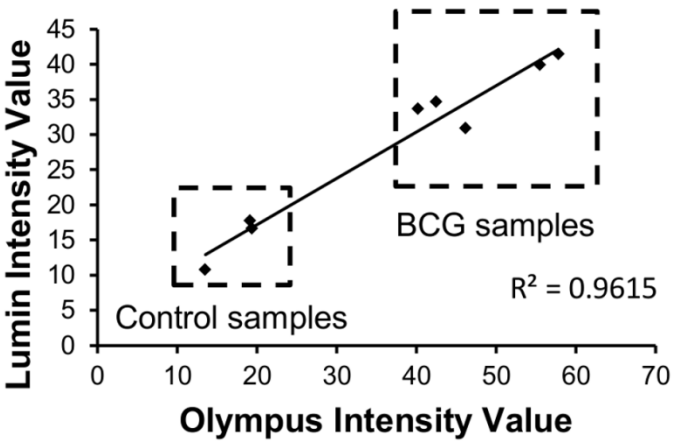

Figure 2.7. Preliminary comparison between Olympus and Lumin raw intensity values obtained from microtip measurement. The microtips were evaluated in treated sputum samples spiked with either PBS alone (control) or PBS containing BCG cells at 10^4 CFU/mL.

2.3 Discussion

There are various techniques for processing sputum, however, these sputum processing protocols focus on either (i) killing all organisms other than *M. tuberculosis* for isolating and culture [69-72] or (ii) extraction of mycobacterial DNA for molecular diagnostic studies [73-75]. The first set of protocols does not disinfect all organisms and cannot be directly used. The second set completely kills and renders the cells noninfectious; however, the cells are lysed in the process to release the DNA. The microtip sensor uses an electric field to generate dielectrophorectic (DEP) forces to concentrate MTB to the microtip from a large volume solution. This force requires intact cell membrane and wall structures (this phenomenon will be covered in chapter 3); thus protocols used for extraction of DNA cannot be applied due to cell lysis.

In the present study, heating to 60°C for 5 to 10 minutes in the presence of 1 M NaOH and 1% SDS was sufficient to kill the cells by a factor of approximately 10^6-fold while being captured with DEP. Because heat transfer can vary depending on equipment and labware, a 10 minute heat treatment was used to confer a margin of error. We hypothesize that our method exploits the reversible phase shift of the mycobacterial cell wall that occurs at around 60°C [64]. Heating to the transition temperature may reduce the cell's structural resistance or resilience in the face of chemical challenges.

Previous observations found that high temperatures were needed to inactivate *M. tuberculosis* in the absence of chemical challenges. Zwadyk and colleagues [73] reported 50% inactivation after 95°C in a dry heat block for 20 minutes. Bemer-Melchior and Drugeon reported 20% inactivation after 20 minutes at 80°C [76]. However, Doig and colleagues reported that heating to 80°C for 20 minutes fully submerged in a water bath was sufficient to kill all the

cells [77]. In all of these reports, temperatures ≥80°C were required to inactivate significant percentages of *M. tuberculosis* cells. Our results demonstrate that simultaneous exposure to chemical challenges (0.1 M NaOH and 1% SDS) can lower the temperature requirement to 60°C, a level that may in the future enable the use of chemical- or battery-powered heat supplies to render patient samples safe for analysis [78].

Integrity of the surface antigens were a concern after sputum treatment with chemicals and heat. Loss of integrity of antigens could preclude the use of antibody-based detection protocols such as the microtip sensor. To test this possibility, we initially attempted to use an enzyme-linked immune-sorbent assay (ELISA) to characterize antigen integrity after the biosafe treatment. However, the presence of sputum resulted in high background signals regardless of treatment (not shown). Therefore, antigen activity was evaluated by using the immunofluorescent microtip assay. Samples treated by the biosafe method exhibited detection results that were essentially identical to previous results generated by using the NALC method [63]. The assay detected *M. tuberculosis* complex cells with a limit of detection of approximately 100 CFU/mL, in less than 30 minutes (sample to result), with no cross-reactivity to an unrelated bacterium (*S. epidermidis*) or to other microorganisms present in multiple sputum samples. It cross-reacted with other *Mycobacterium* species, but this appears to be an innate property of the polyclonal antibody, which was raised in chickens against whole acetone-fixed BCG cells [63].

The current configuration of the microtip assay requires fluorescence detection, which can be expensive depending on the instrument used. To determine if the method can utilize inexpensive fluorescence microscopy equipment, we compared fluorescent intensity values obtained by using the battery-powered LED of Lumin fluorescence microscope to those obtained by using the more elaborate and expensive Olympus BX-41 unit. The development of light

emitting diodes (LED) with fluorescent capabilities and low power requirements has led to the recent introduction of robust, inexpensive, battery-powered fluorescent microscopes such as the Lumin instrument [79, 80]. Given that microtip visualization requires modest magnification (20X objective) and uses a well-defined focal plane, we hypothesized that a low-cost instrument could function as well as a high-end one. Although the Lumin's overall raw fluorescence intensity values were lower than those of the Olympus, the results were comparable.

2.4 Summary

An occupationally safe (biosafe) sputum processing protocol was developed for rapid diagnosis of *Mycobacterium* using an updated, semi-automated immunofluorescence-based microtip sensor. A synergistic strategy combining moderate chemical and thermal treatments for 10 minutes inactivated *M. tuberculosis* and other potential pathogens in sputum, while maintaining the integrity of mycobacterial surface antigens. When applied to biosafe-treated samples, the semi-automated microtip immunofluorescence sensor exhibited the predicted specificity and a detection limit of 100 CFU/mL. The detection time from untreated sputum sample to the final results was 30 minutes with analytical sensitivity comparable to commercial PCR [47]. In addition, the device was semi-automated and the protocol was shown to work well with low-cost, LED-powered microscopy. The new device and the biosafe protocol may prove useful in the future for TB diagnosis in settings with limited laboratory infrastructure. However, at this point, the device has yet to be evaluated for drug-susceptibility. To determine if it is possible, a fundamental study on the electrokinetic forces must be undertaken on *Mycobacterium tuberculosis* complex cells.

Chapter 3: Investigation of AC Electrokinetic Forces in Semi-Conductive Buffers

3.1 Introduction

AC electrokinetic techniques, dielectrophoresis (DEP) and AC electroosmosis (ACEO) in particular, have seen an increase in popularity in recent years due to its scalability for miniaturization, with advantages including portability, sample size, and versatility [81-84]. One of the great advantages of DEP is the ability to separate particles depending on their physical and electrical properties. It has been greatly utilized to characterize and separate various biological particles such as bacterial populations [85, 86], mammalian cells [87, 88], DNA [89, 90], and proteins [91]. The separation is caused by the relative differences of electrical and physical properties between the particle and surrounding medium. Under DEP, particles will move towards (positive DEP) or away (negative DEP) from electrode edges where a high electric field gradient is generated. The DEP attraction or repulsion is attributed to the Clausius-Mossotti factor (CM factor, described later). The other electrokinetic technique ACEO is an electrohydrodynamic phenomenon caused by the charge interaction between the electric field and electrical double layer, resulting in a fluid flow over the electrode surface. ACEO has been used for mixing in microchannels [92, 93] and transport [94-96] of submicron particles.

Using microfabricated planar electrodes, high electric fields of 10^4-10^6 V m^{-1} can be achieved with relatively small voltages of AC fields. In comparison, DC electrokinetic techniques such as DC electroosmosis could result in electrolysis of the solution and contaminate

the electrodes. These benefits make AC electrokinetic techniques indispensable for microfluidic devices and lab-chip biosensors compared to other particle manipulation techniques such as optical tweezers [97, 98] and magnetic particles [99].

Previous works utilizing eletrokinetic forces have mainly investigated low conductive media ($< 10^{-3}$ S m^{-1}) to manipulate polystyrene spheres and biological particles. Using low conductive media, the magnitude of DEP force is enhanced; increasing the number of particles attracted and trapped by positive DEP thereby readily distinguishing DEP force. The potential problem with low conductive media for biomedical applications is that biological samples are suspended in highly conductive media (> 1.0 S m^{-1}). To reach the low media conductivity, the samples would need to be diluted or centrifuged several times with deionized water. The process is cumbersome and importantly, may not be possible for some biological particles due to potential damage of target particles. The detection limit can be worsened with the dilution. Additionally, the use of low conductive buffers results in high mortality rate of microorganisms due to osmotic stress.

An alternative approach is to use high conductive media (> 1 S m^{-1}) and trap particles by negative DEP [100-103]. Increasing the conductivity of the media eventually switches the DEP from positive to negative; repelling particles away from electrode edges with high electric field gradients and concentrating particles in low field regions. By doing so, assays would be able to use physiological buffer conditions and be functional for biological applications. The drawbacks of using such a system include possibility of sample heating, electrochemical damage, and the repulsion of cells away from electrodes makes cell trapping more difficult in a continuous flowing microfluidic system. Lastly, negative DEP overlooks the very interesting CM factor extracted from the complex conductivity and permittivity of the different layers in a cell

(membrane, cytoplasm), making it insensitive in differentiating slightly altered cells. This will be discussed in Chapter 4.

In this chapter, we propose the use of a semi-conductive media (0.07 S m^{-1}) and investigate the electrokinetic forces coexisting in the system. A semi-conductive media can combine the advantages of both low and highly conductive setups previously mentioned. It can be easily prepared while retaining positive DEP to effectively trap cells depending on their electrical properties. The system however, is more complex where it must consider the augmentations of DEP caused from electrohydrodynamic flow, mainly ACEO. Unlike previous works implementing low conductive medium which can easily distinguish positive DEP, the rise in conductivity reduces the magnitude of DEP force and may be overpowered by the fluid flow from ACEO. Both ACEO and DEP are a function of frequency, thus the system must be optimized by determining the ideal frequency to generate enough ACEO to effectively deliver cells to the planar electrode gap without overcoming the DEP force to retain the cells on the edge. This chapter presents numerical and experimental study conducted on a simplified isolated planar electrode to investigate the combined effects of DEP and ACEO. Additionally, *M. bovis* BCG cells are used in this study, which previously has never been investigated for electrokinetic techniques. The presented analysis will give insight on the properties of *Mycobacterium* cells, as well as evaluate if our microtip biosensor is capable of drug-susceptibility tests.

3.2 Theory of Electrokinetics

3.2.1 Dielectrophoresis

DEP was first discovered and investigated five decades ago by Pohl in 1951 and later applied to bacteria separation in his lab in 1978 [104] using only few platinum wires on a microscope slide [105]. Since then, it has grown and been applied to detection and manipulation of various types of cells and organisms [85-91].

DEP has seen a large increase in interest in the last decade due to advancement of technology in microfabrication and microfluidic systems. Micro- and nano-sized electrode arrays necessary for electrokinetic forces such as DEP can be fitted into more complex microfluidic systems to achieve selective separation and manipulation of cells. According to scientific data bases of ScienceDirect, Web of Science, etc, there have been 700 publications related to DEP in the last decade. New studies on experimental methods and applications are being discovered because the various electrical and physical properties of cells can greatly affect DEP functions. Therefore, to achieve the desired cell manipulation using DEP for a specific system, it is essential to understand the DEP in relation to the electrical properties of the particle and suspending medium.

DEP is the motion of polarized particles subjected to a non-uniform electric field due to the interactions of the particle's induced dipole under gradients of the electric field. When a dielectric particle such as a cell is suspended in liquid media and subjected to a non-uniform electric field, the particle becomes polarized. This process is known as Maxwell-Wagner interfacial polarization. The polarization is from the movement of free charges and field-induced perturbation of bound charges.

For a homogeneous spherical particle, the net force F_{DEP} for a particle with equivalent radius r is given by [106]:

$$F_{DEP} = 2\pi r^3 \varepsilon_m \mathrm{Re}[K(\omega)] \nabla |E_{rms}|^2, \quad (3.1)$$

where ε is the permittivity of medium and E_{rms} is the root mean-square electric field. The factor $K(\omega)$ is the Clausius-Mossotti (CM) factor, which depends on the complex permittivity (ε^*) of the particle (p) and medium (m) and given by:

$$K(\omega) = \left(\frac{{\varepsilon_p}^* - {\varepsilon_m}^*}{{\varepsilon_p}^* + 2{\varepsilon_m}^*} \right), \; \varepsilon^* = \varepsilon - \frac{j\sigma}{\omega} \quad (3.2)$$

where ω is the angular frequency of the applied field ($\omega = 2\pi f$), $j = \sqrt{-1}$, σ is the conductivity, and ε the permittivity.

For the complex permittivity, the polarization and CM factor are dominated by conductivity at low frequencies. As the frequency increases, however, the permittivity becomes more dominant. The reason is that there is a limit on how fast ions can be conducted across the material where at higher frequencies the ions will not have enough time to respond.

The CM factor determines the direction the particle will move towards. When particles are more polarizable than the surrounding medium, i.e., $\mathrm{Re}[K(\omega)] > 0$, particles will move toward the region with maximum electric field. This phenomenon is called positive DEP. Alternatively, when the medium is more polarizable than the particles, i.e., $\mathrm{Re}[K(\omega)] < 0$, the particles will be repelled and move towards the region with minimum electric field. This is called negative DEP. The transition frequency where the behavior switches from positive DEP to negative DEP or vice versa is known as the crossover frequency (cof). The cof is experimentally

significant because it depends on the relative difference of the electrical properties between the particle and medium; which can be used to estimate the particle's electrical properties. This will be discussed further in the later sections.

Biological cells, however, are more complex and far from homogeneous. They can have cell membranes and walls and cytoplasm with a nucleus. Irimajiri *et al*. [107] simplified the cell by developing a "multi-shell" model. This model assumes a homogeneous particle surrounded by a medium with a finite thickness, which is then surrounded by another medium, each with electrical properties. The CM factor for a multi-shell particle can be obtained by estimating an effective complex permittivity and conductivity, where each layer is progressively merged together. This method was formulated by Huang *et al*. [108]. For a single-shell model:

$$\varepsilon_p{}^* = \varepsilon_{mem}{}^* \left[\frac{\left(\frac{R}{R-d}\right)^3 + 2\left(\frac{\varepsilon_{cyto}{}^* - \varepsilon_{mem}{}^*}{\varepsilon_{cyto}{}^* + 2\varepsilon_{mem}{}^*}\right)}{\left(\frac{R}{R-d}\right)^3 - \left(\frac{\varepsilon_{cyto}{}^* - \varepsilon_{mem}{}^*}{\varepsilon_{cyto}{}^* + 2\varepsilon_{mem}{}^*}\right)} \right], \tag{3.3}$$

where the effective complex particle permittivity $\varepsilon_p{}^*$ is composed of the complex permittivity of cytoplasm (cyto), cell membrane (mem), outer cell radius (R), and membrane thickness (d). The effective complex particle permittivity is substituted into Eqn. 3.2 to obtain the multi-shell CM factor.

Cells such as *E. coli* and *Mycobacterium* are even more complex because they are not round but rod-shaped. Additionally, they still consist of a cytoplasm membrane and a cell wall which will require a multi-shell model as depicted in Fig. 3.1. The CM factor must be adjusted for the new geometry of an ellipsoid spheroid. This new CM is expressed as [106]:

$$K_i(\omega) = \frac{1}{3}\left(\frac{{\varepsilon_p}^* - {\varepsilon_m}^*}{{\varepsilon_m}^* + A_i({\varepsilon_p}^* - {\varepsilon_m}^*)}\right), \qquad i = x, y, z \tag{3.3}$$

where A is the depolarization factor along one of the three axes [109]. The depolarization factor for the major axis in the x direction is given by:

$$A_x = \frac{1 - e^2}{2e^3}\left[\log\left(\frac{1+e}{1-e}\right) - 2e\right], \qquad e = \sqrt{1 - \left(\frac{b}{a}\right)^2} \tag{3.4}$$

With e being the eccentricity and a and b are the radii of a prolate spheroid ($a > b$). The minor axis's depolarization factor has the same value due to symmetry of the ellipsoid, and given as:

$$A_y = A_z = \frac{1 - A_x}{2}, \tag{3.5}$$

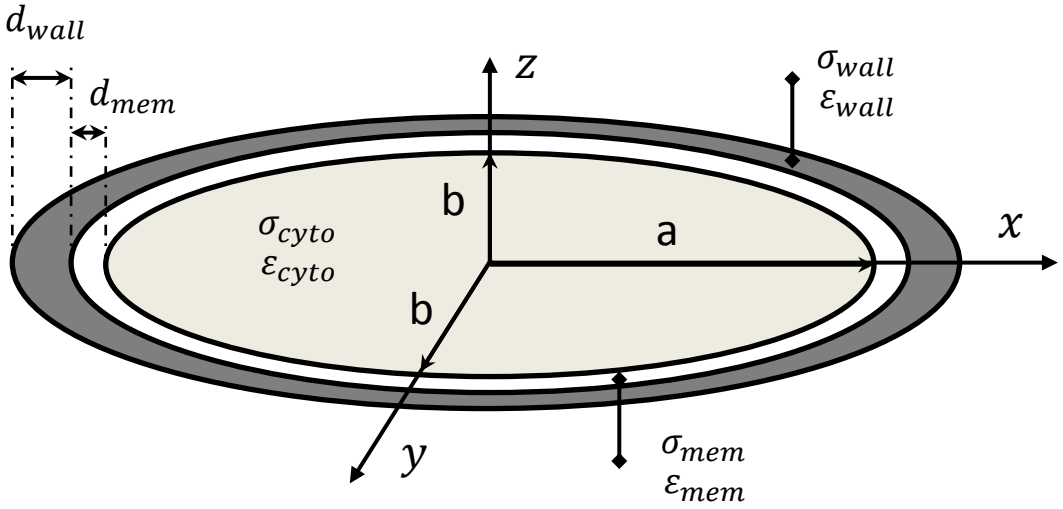

Figure 3.1. Depiction of double-shell model of a cell with a membrane and wall, each with their respective thickness of d, conductivity σ, and permittivity ε.

Expanding this to multi-shell system is very complex, but Huang *et al.* [110, 111] has provided a complete analytical expression of a prolate (rod-shaped) spheroid for a single wall which can then be expanded to multiple layers. The $K_i(\omega)$ for a single-shell prolate spheroid is found by:

$$K_i(\omega) = \frac{1}{3}\frac{(\varepsilon_{mem}{}^* - \varepsilon_m{}^*) + 3K_{cyto,i}\rho\left[\varepsilon_{mem}{}^* + A_{mem,i}(\varepsilon_m{}^* - \varepsilon_{mem}{}^*)\right]}{\left[\varepsilon_m{}^* + A_{mem,i}(\varepsilon_{mem}{}^* - \varepsilon_m{}^*)\right] + 3K_{cyto,i}\rho A_{mem,i}(1 - A_{mem,i})(\varepsilon_{mem}{}^* - \varepsilon_m{}^*)}, \quad (3.6)$$

where $i = x, y, z$. The depolarization factor A is the same, however, the eccentricity changes to:

$$e = \sqrt{1 - \left(\frac{b + d_{mem}}{a + d_{mem}}\right)^2}, \quad (3.7)$$

to account for the distance change. Approximating the layer to be a constant, the volume ratio between these layers is then:

$$\rho = \frac{a \cdot b^2}{(a + d_{mem}) \cdot (b + d_{mem})}, \quad (3.8)$$

The DEP profile can then be solved by averaging the CM factor from each axis. A DEP response for the double shelled, ellipsoid CM factor is shown in Fig 3.2.

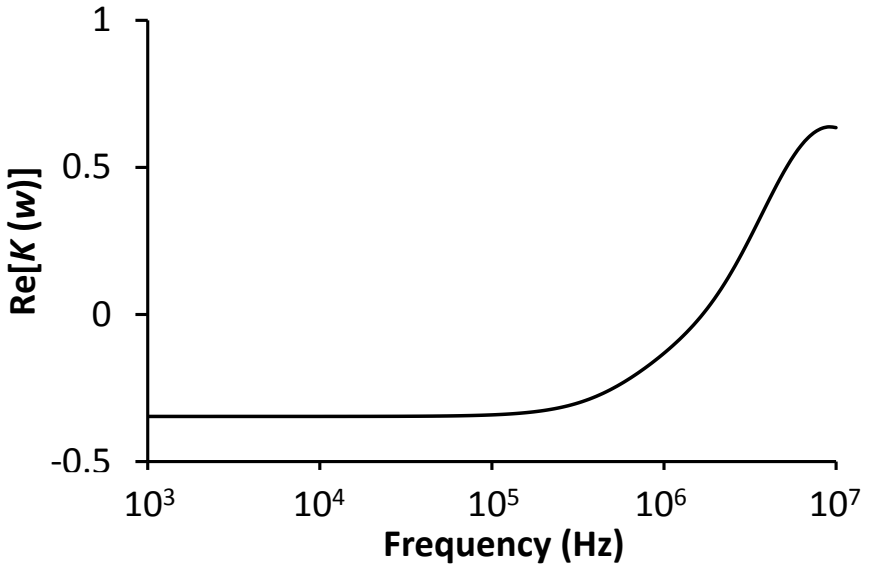

Figure 3.2. DEP response of a double-shelled ellipsoid. As the frequency increases, the CM factor changes from negative to positive DEP. The transition point is the crossover frequency (cof).

3.2.2 AC electroosmosis

AC electroosmosis is gaining more ground compared to its counterpart of DC electroosmosis due to the less contamination on electrode surface. The physics behind both is different in that DC electroosmosis relies on the static charges while AC electroosmosis induces frequency-dependent surface charges in the diffuse double layer by applying voltage. One form of fluid velocity v from DC electric field is found to be [112, 113]:

$$v = \frac{E_t \sigma_q}{\kappa \eta}, \tag{3.9}$$

where E_t is the tangential electric field, σ_q is the surface charge density in the diffuse double layer, κ is the reciprocal Debye length, and η the fluid viscosity. In a nonuniform electric field,

E_t lies tangential to the electrode surface and the charge in the diffuse double layer can be represented as a time dependent excess charge $\Delta\sigma_q$ where it can be estimated to be $\Delta\sigma_q = \varepsilon\kappa V_d$ with ε as the permittivity of the medium and V_d is the induced potential across the double layer.

For AC voltages, the double layer polarization effects will make the magnitude of E_t and $\Delta\sigma_q$ frequency dependent [114, 115]. At low frequencies, the applied voltage will be almost entirely be dropped across the double layer whereas at higher frequencies the potential drop across the double layer goes to zero due to polarization of the electrode/solution interface. Thus AC electroosmosis will cease at low and high frequencies.

Further analysis was performed by Ramos and colleagues using a circuit model to give the frequency dependence of V_d with the velocity profile across the electrode [112, 116]. The fluid velocity at the electrode surface at distance z is

$$v = \Lambda \frac{1}{8} \frac{\varepsilon V_o^2 \Omega^2}{\eta z (1+\Omega^2)^2}, \tag{3.10}$$

where V_o is the voltage amplitude, Λ is the ratio between the Stern and diffuse double layer capacitance given as

$$\Lambda = \frac{C_s}{C_s + C_d}, \tag{3.11}$$

and Ω is the nondimensional frequency given as

$$\Omega = \omega \frac{\epsilon}{\sigma} \frac{\pi}{2} z\kappa, \tag{3.12}$$

where ω is the angular frequency. Eqn. 3.10 gives a bell-shaped velocity profile with respect to frequency, where low and high frequencies tend to zero velocity (Fig 3.3). This equation also

shows that the frequency for the maximum velocity should increase as the medium conductivity increases.

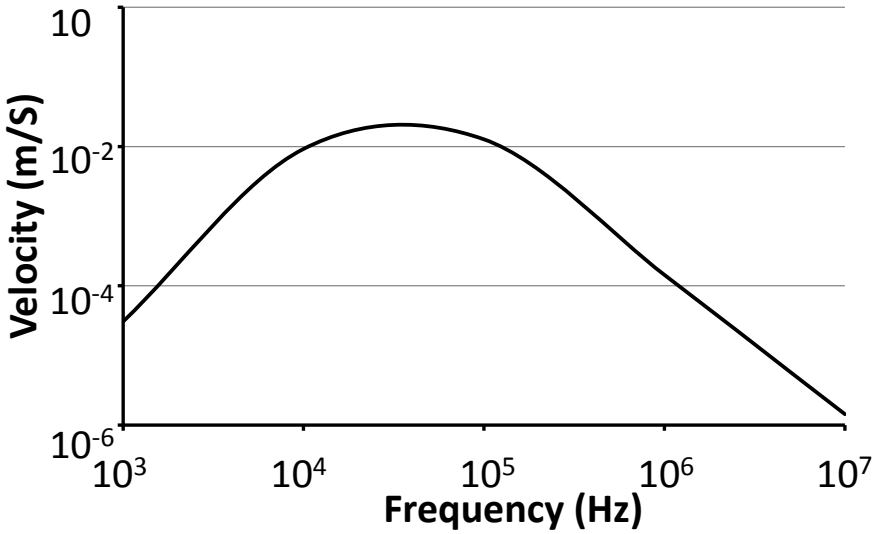

Figure 3.3. Velocity profile from ACEO ($\boldsymbol{\sigma_m = 0.07}$).

3.2.1 Electrothermal flow

Electrothermal flow is another electrokinetic phenomenon but will not be discussed in depth in this paper. Electrothermal flow is caused by temperature gradients induced from joule heating. The temperature gradient in turn creates fluctuations in the conductivity and permittivity of the fluid resulting in fluid motion. In general, higher conductive media (> 0.2 S m^{-1}) and applied voltage leads to electrothermal flow due to higher heat generation. Electrokinetic assays implementing high media conductivity to transport or concentrate particles explore this phenomenon. Electrothermal flow, however, is usually insignificant compared to ACEO. Only

when media conductivity is increased to where electrical double layer becomes significantly suppressed and high thermal gradients are present (> 1 S m^{-1}) do they become significant [100, 117, 118]. Our configuration used 0.07 S m^{-1} and applied voltage of 20 $V_{p.p.}$. In this experimental condition, fluid motion was not observed at 10 MHz. At this medium conductivity, voltage, and frequency, ACEO should become suppressed and any residual flow would be caused by electrothermal effect; however, since there was no flow present, electrothermal flow in the system is insignificant. Therefore this paper will not discuss this flow mechanism.

3.3 Materials and Methods

3.3.1 Planar electrode fabrication

Planar electrodes were fabricated in microfabrication laboratory (Washington Technology Center, University of Washington). Low pressure CVD was used to grow 300 nm of oxide layer on the silicon wafer. Chrome and gold layers were then evaporated onto the surface using e-beam evaporator. Electrodes with gap size of 10 μm were patterned onto the silicon wafer using conventional photolithography. The patterned wafer was then placed in gold and chrome etchant to remove the unwanted layers. Figure 3.4.a shows a completed planar electrode chip.

3.3.2 BCG culture

BCG used in this study was cultivated in a shaker at 37°C. BCG were cultured in Difco Middlebrook 7H9 Broth (BD Diagnostics, Sparks, MD) supplemented with 10% (v/v) ADC enrichment and 0.05% Tween 20. The bacterial culture was conducted in Cangelosi's laboratory at University of Washington.

3.3.3 Cell preparation

100 μL of 10^8 CFU/mL BCG cell suspension [based on optical density (A_{600}) measurements] in 7H9 culture broth was diluted 1:10 in deionized water (DI) to obtain 1 mL of 10^7 CFU/mL. The cells were stained with Live/Dead *Bac*light kit (Invitrogen, Carlsbad, CA) for labeling and left at room temperature for 15 minutes prior to experimentation.

3.3.4 Experimental setup

A planar gold electrode with a gap length of 10 μm was used to characterize the electrokinetic responses of BCG cells. The electrodes were connected to a function generator (Agilent 33220A, Santa Clara, CA) with a frequency ranging from 1 kHz to 10 MHz for 1 minute. The voltage applied was 20 $V_{p.p.}$, except for frequencies of 1 kHz and 10 kHz where 6 $V_{p.p.}$ and 12 $V_{p.p.}$ were used, respectively. At lower frequencies, the voltages needed to be lowered to prevent electrolysis in the solution. A fluorescent microscope (Nikon Eclipse 55i) recorded and imaged the cells after 1 minute. A depiction of the setup is shown in Figure 3.4.b.

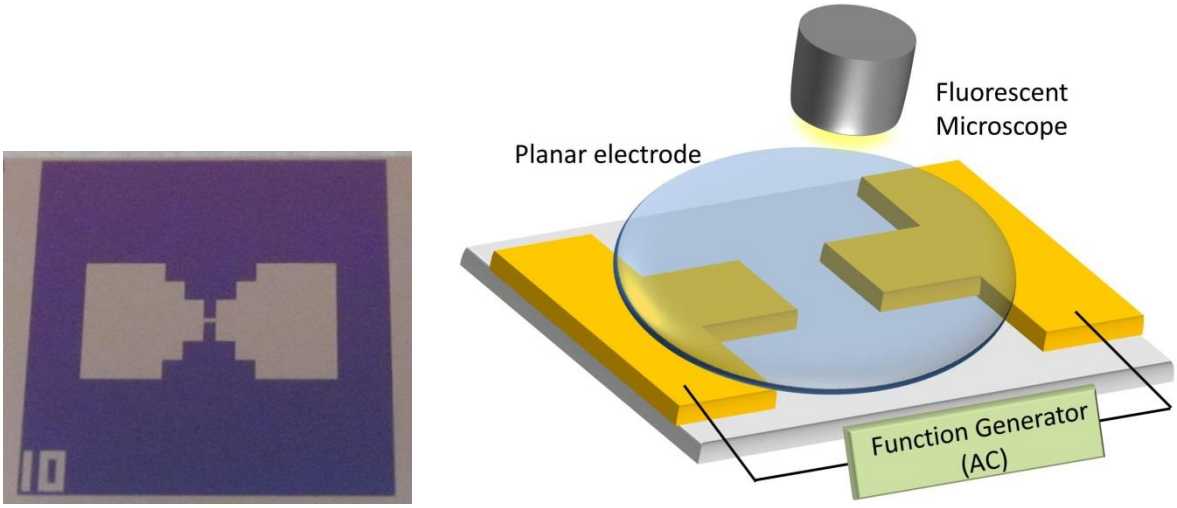

(a) (b)

Figure 3.4. (a) Fabricated planar electrode with a gap size of 10 μm. (b) Illustration of experimental setup.

3.3.5 Simulation

Simulation is used to predict the behavior of particles after experiencing the electrokinetic forces due to DEP and ACEO. The total force F_{tot} is calculated by:

$$F_{tot} = F_{DEP} + F_{Drag}, \tag{3.13}$$

where F_{Drag} is the drag force from ACEO. Brownian motion has been excluded due to the micrometer size of particles, which makes Brownian motion negligible. The gravitational force is also omitted because the density of the cells is comparable to that of the solution. The drag force is from the relative motion of the particle under the flow, and given by:

$$F_{Drag} = -6\pi\eta r\left(\frac{\Delta x}{\Delta t} - u\right), \tag{3.14}$$

where η is the viscosity of the medium, r is the particle radius, x is the particle displacement, t is the time, and u is the flow velocity. Since the particle is very small, the time to reach terminal velocity is orders of magnitude different with respect to the time step of the simulation. Therefore, it is assumed that there is no acceleration and the total net force acting on the particle is zero [119]. The simulation was done by computing for particle position x using COMSOL Multiphysics. Note that the numerical simulation was completed with the assistance of Hyun-Boo Lee.

3.4 Results

Electrokinetic responses of stained BCG cells for various frequencies in a semi-conductive media were investigated. Cell suspension of 2 μL was exposed to frequencies ranging from 1 kHz to 10 MHz on a planar electrode for a period of 1 minute as seen in Fig 3.5. Frequencies below 1 kHz were not evaluated because any lower frequencies resulted in damaging of the electrodes. Frequencies higher than 10 MHz were not evaluated due to the limitation of a function generator where the high frequency limit was 20 MHz.

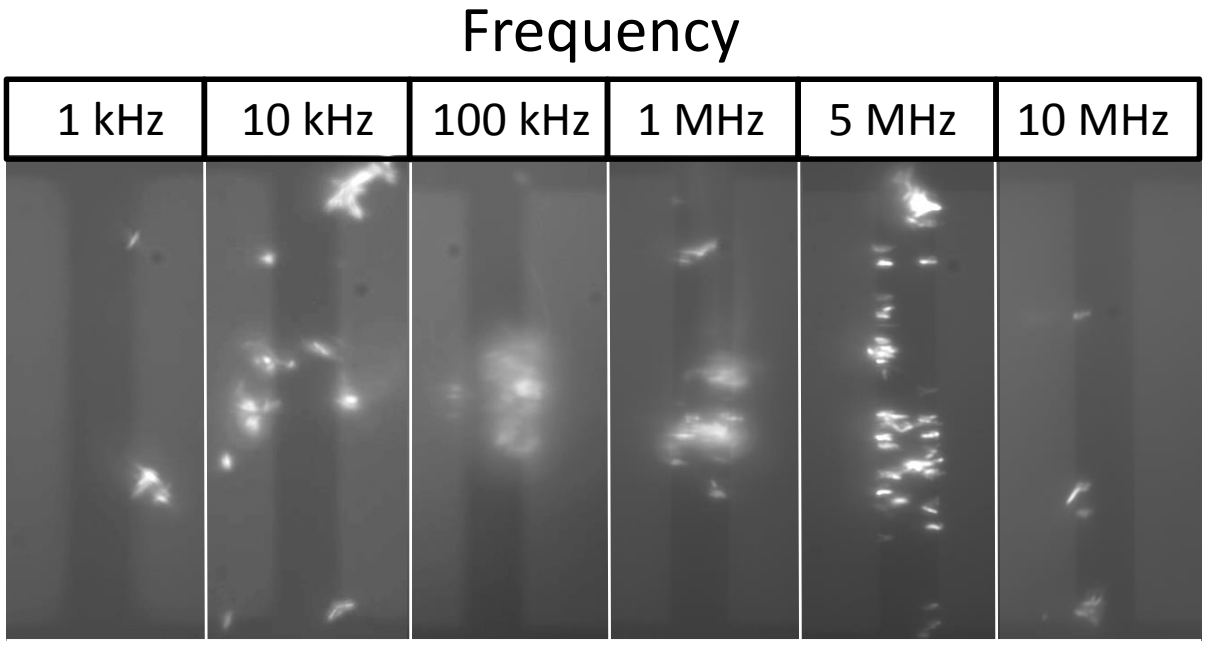

Figure 3.5. BCG cells attracted to planar electrode gap after 1 minute at frequencies ranging from 1 kHz to 10 MHz.

Frequency of 1, 10, and 100 kHz showed a noticeable trend. As the frequency increased from 1 to 100 kHz, the cells' velocity gradually increased and was the highest near the electrode edge. As the cells were attracted to the gap, they could be seen vortexing around the edge and

progressively moving toward the center of the electrode. The cells moving faster than others were projected back into the suspension. As the frequency and velocity increased, more cells were captured in the vortex. This vortex was observed to be getting smaller as frequency increased. The trend is shown in Fig 3.6. At this point, cells were trapped in the fluid vortex but not immobilized onto the electrode edges.

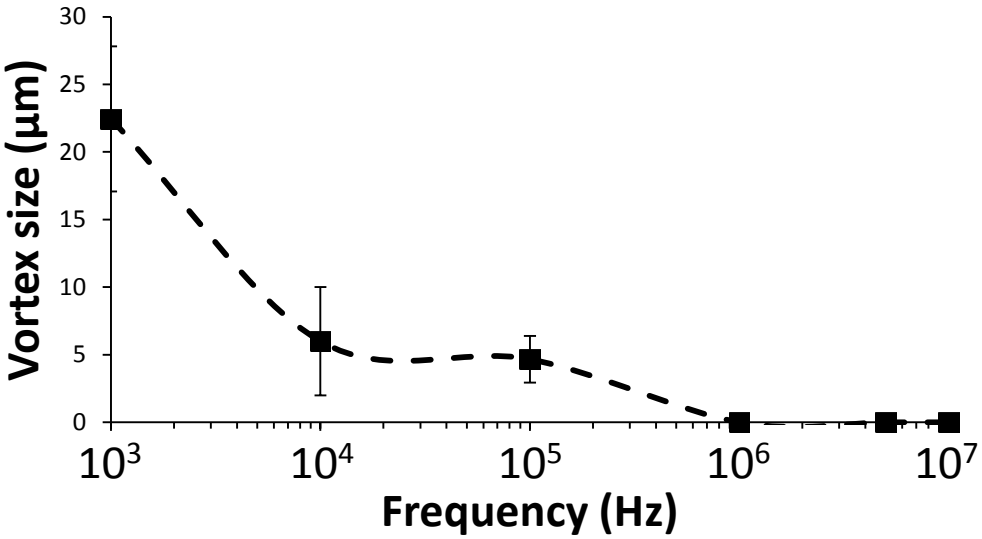

Figure 3.6. Vortex size depending on the frequency of an applied voltage between two electrodes having 10 µm in gap size.

Beginning from 1 MHz, cells started showing a decrease in velocity and began to be immobilized between the electrode gaps. However, some cells that were attracted towards the electrode edge were not complexly immobilized and could be seen sliding up and down the gap length. The size of the vortex was no longer visible as other cells which were not captured glided across the electrode surface and not upward back into the suspension.

The movement of the cells for 5 MHz was more limited than at 1 MHz, however, the number of cells pulled down from the solution into the gap was still high. Additionally, most

cells that approached the gap were completely immobilized and did not shift along the edges. 5 MHz showed the highest number of immobilized cells on the electrode.

The high frequency of 10 MHz immobilized all the cells that approached the gap; however, fluid flow was negligible. Without the fluid flow, only the BCG cells that were immediately in the vicinity of the edge approached the electrode. After the allocated period of 1 minute, only a few cells were captured in the gap.

Fig. 3.7 shows the number of immobilized BCG cells on the planar electrode gap after 1 minute. It was found that 5 MHz had the highest number of cells, then 1 MHz and 10 MHz. The frequencies from 1 to 100 kHz might have attracted cells, but cells which were stuck in the fluid vortex were not counted.

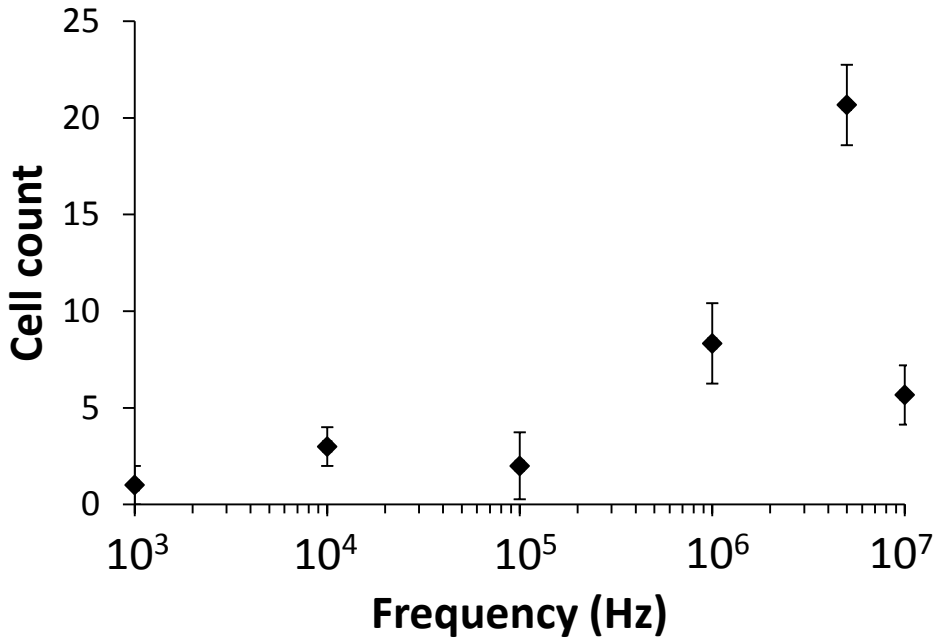

Figure 3.7. Cell count under the frequency ranging from 1 kHz to 10 MHz.

3.5 Discussion

3.5.1 Separating ACEO and DEP

ACEO and DEP were first analyzed separately using the numerical simulation to understand to what degree each phenomenon affects the BCG cells. We can then integrate the forces numerically and compare with the experimental results.

The analytical equation of ACEO from Eqn. 3.10 produced a bell curve (Fig 3.3) where fluid flow was highest for 10 and 100 kHz, and declined towards 1 kHz and 1 MHz with 10 MHz being the lowest. The experiment followed a similar trend where fluid flow increased from 1 kHz and was most dominant for 10 and 100 kHz. It then declined until 10 MHz where flow was not observed. Since the trend follows, it is conservative to assume that the fluid flow in this system is dominated by ACEO.

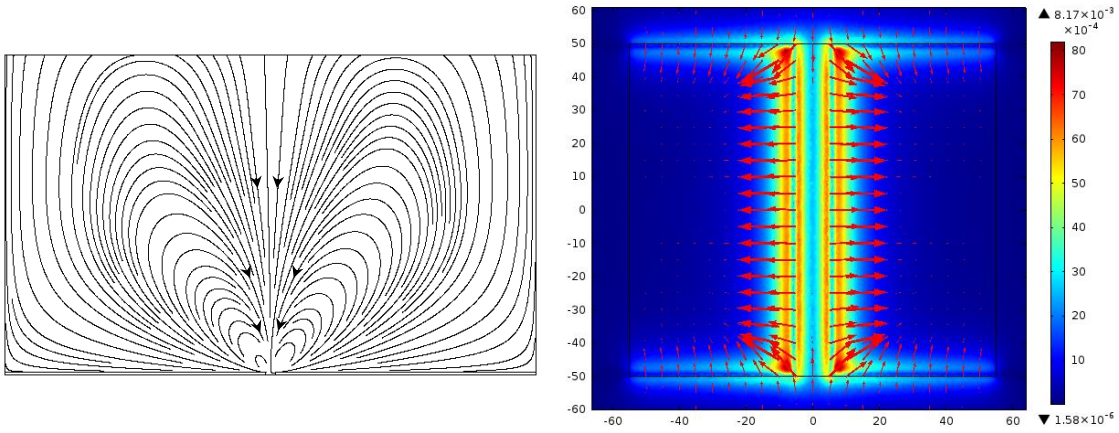

Figure 3.8. Numerical results for ACEO flow (a) Streamline from the side profile of the electrodes (b) Fluid flow due to ACEO from the top view.

Simulations of the flow streamlines and flow vectors/velocity magnitudes from ACEO are shown in Fig 3.8. In Fig 3.8.a, the streamline from the side profile shows vortices emanating

from the electrode gap. The vortex flows from the center of the gap then across the surface of the electrode and circulates back towards the gap. As cells approach the electrode gap, the slip velocity generates a fluid flow creating a vortex. The top view (Fig 3.8.b) shows the flow vectors, and flow velocity magnitudes are high at the edges and highest at the corners of the electrode. This implies that the velocity is highest as the distance between the particle and electrode surface decreases. Experimental results showed similar movement of cells as they approached the edge of electrodes and indicates that the flow is generated in this region, which is consistent with the numerical result of ACEO driven by the electrical double layer. Additionally, the existence of a higher velocity magnitude from the corners of the electrode will concentrate cells towards the center of the gap. This effect was prevalent from 1 kHz to 1 MHz, where the cells slowly migrated towards the center. For 1 MHz, this flow caused the partially immobilized cells to shuffle up and down the edge of the gap.

The streamline in Fig 3.8.a can be seen to extend relatively far into the suspension. This is necessary to concentrate the cells and increase the effective sensing area. This flow pattern was consistent with the vortices of 1, 10 and 100 kHz. As the vortices formed, cells were pulled down from the suspension and concentrated in the vortex. The vortex, however, became smaller and smaller until it was not noticeable after 100 kHz (Fig 3.6). It has previously been reported that the size of the vortex decreases as the frequency increases and center of vortex approaches the electrode edge [116]. The disappearance of the vortex, however, did not stop the fluid movement. Even without the vortex, the flow pattern remained similar where cells were pulled down to the gap but instead of flowing upwards back into the suspension, it flowed parallel to the electrode surface. This new flow may have been due to the removal of the vortex as well as the generation of positive DEP. In fact, removal of the vortex was advantageous because of the

higher fluid velocity near the vortex could eliminate immobilized cells on the electrode edge retained from positive DEP. This was the case for 1 MHz, where cells could be seen to be only partially immobilized but not strong enough positive DEP to withstand the fluid flow.

Previous works have shown the CM factor's cof from negative to positive DEP for *E. coli* [106] and *M. smegmatis* (an easier to culture family of *Mycobacterium*) [82] cells were near 1 MHz. BCG, a bacterium similar to these cells, is thus expected to follow a similar CM factor. Counting of immobilized BCG cells (Fig 3.7) showed that positive DEP was generated at 1 MHz as expected but 5 MHz had the highest capture rather than 10 MHz. Although a high positive DEP force was predicted at 10 MHz by the numerical results, the counting at 5MHz showed a higher yield than that of 10MHz. To understand the reason, the combined effect of DEP and ACEO was investigated.

3.5.2 Combining electrokinetic forces

ACEO and DEP are both electrokinetic phenomena dependent on frequency as seen with fluid velocity and CM factor. To quantify the relationship, Fig. 3.9 shows the estimated F_{DEP} and F_{Drag} from ACEO with respect to frequency. F_{DEP} was calculated using the CM factor derived from the estimated cof of 1 MHz. The estimated properties are listed in Table 3.1. The values are comparable to *M. smegmatis* [82].

Table 3.1. Estimated electrical properties of *M. bovis* BCG using the cof of 1 MHz

$\sigma_{wall}\left(\frac{S}{m}\right)$	ε_{wall}	$\sigma_{mem}\left(\frac{S}{m}\right)$	ε_{mem}	$\sigma_{cyto}\left(\frac{S}{m}\right)$	ε_{cyto}
0.001	**45**	**1E-6**	**20**	**0.5**	**70**

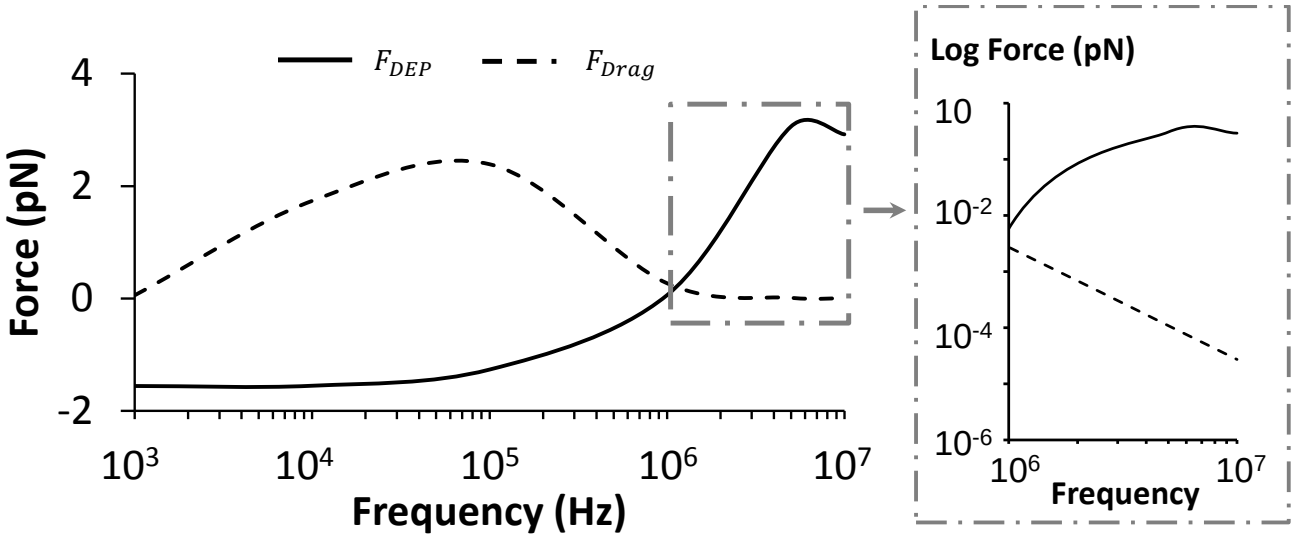

Figure 3.9. DEP and drag forces with respect to frequencies from 1 kHz to 10 MHz. The grey area is shown with logscale of log force (pN) *vs* frequency.

Figure 3.9. shows why 5 MHz captured cells more efficiently than 1 and 10 MHz. Although the flow at 1 MHz is higher allowing for more cells to approach the gap, the drag and DEP forces were comparable. This resulted in cells shuffling and being removed from the electrode edge, effectively reducing the capturing efficiency. 10 MHz and 5 MHz had comparable DEP strength; however, 5 MHz had some fluid flow unlike the stagnant 10 MHz. The drag force was calculated from the analytical equation of ACEO which showed flow around 10~100 μm s^{-1} for 5 MHz. In Eqn. 3.6, the velocity (and thus the force) of ACEO is proportional to $\frac{V^2}{r}$, but DEP has been shown to be proportional to $\frac{V^2}{r^3}$ [118]. Therefore fluid flow played a pivotal role in the capturing because DEP strength diminished exponentially as distance between the particle and electrode edge increased. Since 10 MHz had no ACEO, the effective range of DEP was severely limited, resulting in 5 MHz being the optimal frequency to capture BCG cells in an allocated time. Fig. 3.10 summarizes the fluid flow and DEP interaction on the cells.

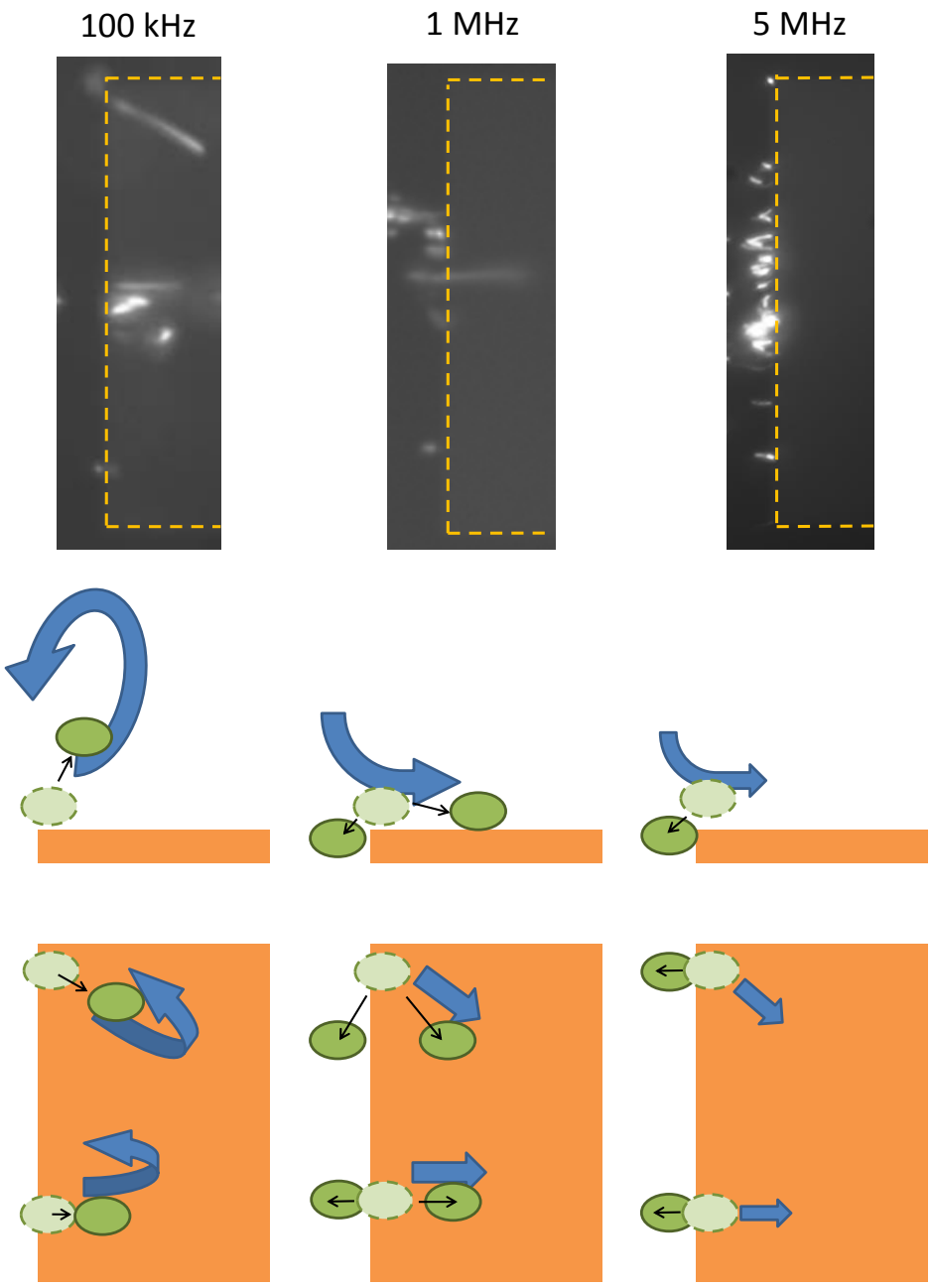

Figure 3.10. Cell behavior under fluid flow and DEP at critical frequencies of 100 kHz, 1 MHz and 5 MHz. The top images show the experimental results of cells at critical frequencies. The schematics represent the expected fluid flow from ACEO and particle movement, with blue arrows representing ACEO flow.

3.5 Summary

In this chapter, we have analyzed the electrokinetic forces of AC electroosmosis and dielectrophoresis effect on *M. bovis* BCG in a semi-conductive buffer. By using an isolated planar electrode, the crossover frequency was estimated to be around 1 MHz. This was the first time BCG cell's properties have been characterized by DEP.

Additionally, we have determined the optimal frequency of 5 MHz to capture BCG cells for analysis. Prior to the cof of 1 MHz, cells were not captured due to negative dielectrophoresis and high fluid force from AC electroosmosis. The cells were repelled from the edges and exerted into the vortex above it. At the cof of 1 MHz, the dielectrophoresis and AC electroosmosis forces were similar, resulting in partial capturing of the cells concentrated by AC electroosmosis. The high frequency of 10 MHz ceased AC electroosmosis flow thereby greatly reducing the capturing distance to the immediate vicinity of the electrode edges. 5 MHz demonstrated the optimal combination of AC electroosmosis and dielectrophoresis for high sensitivity. Based on the numerical and experimental results, heat-killed and drug-killed *Mycobacterium* cells will be differentiated in the next chapter.

Chapter 4: Study of Dielectrophoretic Characterization on *M. tuberculosis* Complex Cells

4.1 Introduction

Differentiation of viable and non-viable cells has much significance in drug-susceptibility and drug-efficacy tests. Current methods mostly rely on culture with direct counting of cells to determine viability [120], which may take time. In microbiology, the distinction between "viable" and "non-viable" cells can be vague [60,61]. Viable usually refers to cells that are able to be cultured; able to divide, multiply, colonize, and overall seem alive. The term non-viable might then refer to cells that are unable to be cultured or grow thus assumed to be dead; however, that is not always the case. Cells may actually be alive and in a dormant state where they are intact but do not multiply. They can defensively remain quiet while in a non-favorable environment, such as with drugs in the system. When the cells are introduced in a more favorable condition, the viability may be recovered. This is one of the ways drug-resistant cells such as multidrug resistant TB (MDR-TB) are developed.

To determine if cells are non-viable or drug-susceptible, there are different characterization methods to measure cell viability, each with their own drawbacks. As mentioned previously, cell counting through plate or liquid culture only works for colony forming cells but not dormant cells. Dormant cells also do not work with metabolic stains, since they require cells to be metabolically active to measure. Live/dead staining dyes such as *Bac*light kit works on dormant cells because they stain intact "live" cells one color and lysed "dead" cells another, but

works only when the membrane structure is compromised. Previous works have shown that dielectrophoresis (DEP) methods are no different. Unless the membrane properties are changed, the cells may not be detected by DEP.

DEP's capability of differentiating viable and nonviable heat-killed cells has been extensively studied [108, 121, 122]. Many have used the information from the heat-killed cells to model DEP response to drug-treated cells [81, 83, 123, 124]. These results have shown the DEP response to be mostly sensitive to alterations of the membrane capacitance (membrane thickness, composition, and morphologies) and internal cellular conductivity. However, there has yet to be any DEP studies conducted on *M. tuberculosis* complex cells to determine if DEP-based detection can be developed to test for drug-susceptibility.

In this chapter, the effect of temperature and two key drugs in treating TB (rifampin and isoniazid) are studied on *M. bovis* BCG in terms of the DEP responses. The DEP crossover frequencies are experimentally determined by observing when the cells switch from attraction to repulsion from electrode edges. By doing so, the dielectric properties of the cells are estimated and characterized. The results show that the DEP characterization method matches the heat and drug mechanism of action; heat and isoniazid compromises the cell wall while rifampin affects only the cytoplasm. The non-viable cells are differentiated from control cells using the optimized frequency and medium conductivity of 5 MHz and 0.07 S m^{-1}, respectively. To this end, the findings demonstrate the capabilities of electrokinetic techniques as a rapid drug-susceptibility test for *Mycobacterium tuberculosis* complex cells.

4.2 DEP Crossover Frequency and Medium Conductivity

The crossover frequency is a critical component in estimation of cell properties when using DEP for characterization. At the crossover frequency, DEP switches from negative to positive DEP. This transition state can be easily observed through experimentation utilizing planar electrodes, where at the crossover frequency range, the cell will switch from being attracted/captured (positive DEP) to repelled (negative DEP). This means at that specific frequency, the dielectric properties of a cell matches those of the surrounding medium. If dielectric properties of the medium are known, one can estimate the properties of the target cell with,

$$f_x = \frac{1}{2\pi}\sqrt{\frac{(\sigma_p - \sigma_m)(\sigma_p + 2\sigma_m)}{(\varepsilon_p - \varepsilon_m)(\varepsilon_p + 2\varepsilon_m)}}, \tag{4.1}$$

where p and m stands for the particle and the medium, respectively. For cells such as *E. coli* and *M. tuberculosis* complex cells, a double shell model may need to be implemented to include the cell wall, membrane, and cytoplasm for the particle calculation. The method to formulate the effective complex conductivity and permittivity of each layer has been previously discussed in Chapter 3.

There are two crossover frequencies when computing for CM factor for single and double shelled particles. The first crossover occurs at a lower frequency range and governed by the cell membrane [106, 125]. As the frequency is increased, the outer shell structure will be neglected and DEP will be dominated by the cytoplasm properties. This is when the second crossover occurs, typically around 100 MHz. In our previous work in Chapter 3, an upper frequency limit of 10 MHz was implemented, thus only observed the first crossover frequency. Using the

estimated BCG properties obtained from Chapter 3, the DEP response up to 100 MHz is shown in Fig. 4.1.

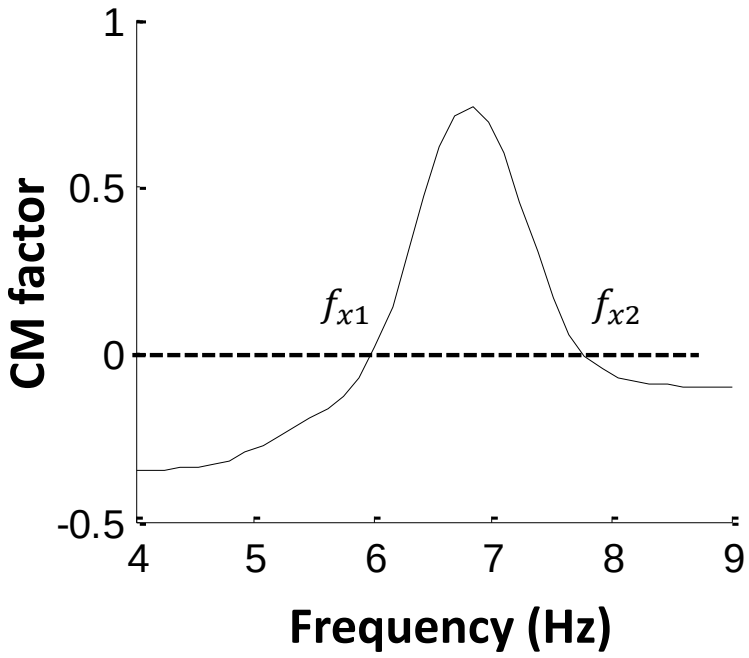

Figure 4.1. CM factor from estimated BCG properties computed in Chapter 3. Increasing the maximum frequency reveals a second crossover frequency, $\boldsymbol{f_{x2}}$.

The medium conductivity has a substantial effect on the first crossover frequency, but not the second crossover frequency. Using the same BCG properties from Fig. 4.1., the effect of medium conductivities can be seen in Fig. 4.2.a. When cells are suspended in low-conductive buffers, cells experience stronger positive DEP, in some cases positive DEP for all frequency ranges (blue line). On the other hand, using highly-conductive buffer produces the opposite effect where negative DEP can be expected for all frequency ranges (red line). Previous works have exploited very low or high conductive mediums to separate cells; however, the first crossover frequency is required to characterize cells. A three-axis map of the crossover

frequency can be generated with relation to medium conductivity using the BCG estimated properties from Chapter 3 (Fig. 4.2.b, c). From the three-axis map, it can be seen that two crossover frequencies can exist from ~10^{-3} to 10^{-1} S m^{-1}.

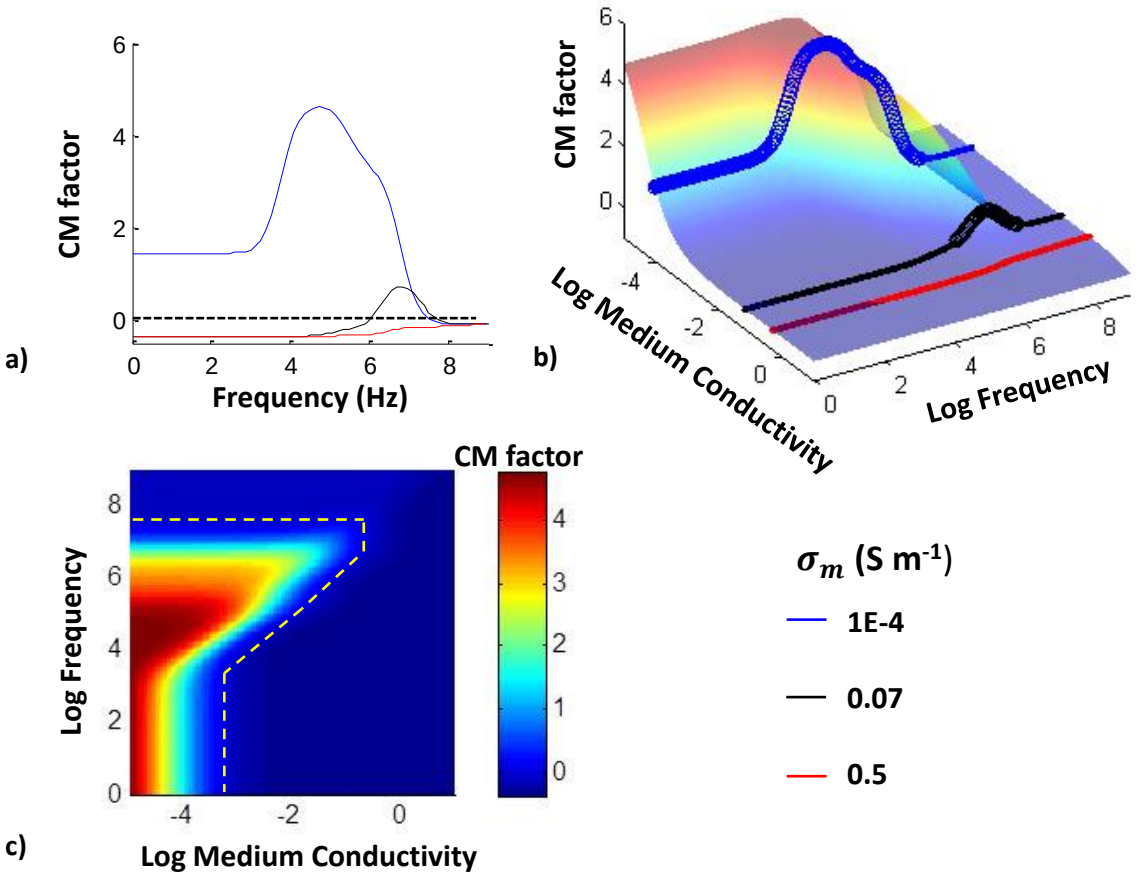

Figure 4.2. Effect of medium conductivity on DEP crossover frequency. a) Estimated properties of BCG cells suspended in low-, semi-, and highly conductive medium. b) Mapping the relationship of crossover frequency with medium conductivity. Thicker lines represent when CM factor is $> \mathbf{0}$. c) Mapping with yellow lines depicting the boundaries of crossover frequency.

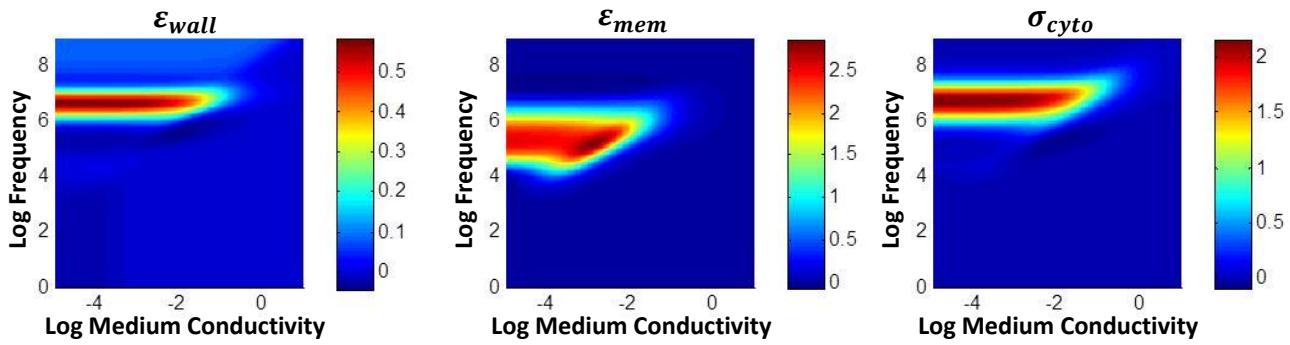

Figure 4.3. Sensitivity of each parameter on crossover frequency. The magnitudes represent how dependent the crossover frequency is to that specific parameter.

Sensitivity analysis was conducted to determine which dielectric parameters were the main variables in affecting the crossover frequency. One parameter was varied while others were fixed to determine the sensitivity. Fig 4.3 shows the first crossover frequency f_{x1} is mainly contributed by the permittivity of the outer shell structure, mainly membrane permittivity (ε_{mem}) at lower frequencies. As the frequency is increased, the permittivity of the cell wall (ε_{wall}) and the conductivity of cytoplasm (σ_{cyto}) has a large effect. The second crossover frequency f_{x2} was highly sensitive to the cytoplasm conductivity. Decreasing the dielectric parameter in each case showed a shift of the crossover frequency to the left (not shown). Therefore, the permittivity of the cells outer structure and cytoplasm conductivity has the largest influence on the crossover frequency.

4.3 Experimental Method

4.3.1 Planar electrode fabrication

Planar electrodes were fabricated in microfabrication laboratory (Washington Technology Center, University of Washington). Thermal oxidation was used to grow 300 nm of oxide layer on the silicon wafer. Gold and chrome was then evaporated onto the surface using e-beam evaporator. Electrodes with gap size of 10 μm were patterned onto the silicon wafer using conventional photolithography. The patterned wafer was then placed in gold and chrome etchant to remove the unwanted layers. Figure 4.4.a shows a fabricated planar-electrode chip.

4.3.2 BCG culture

A stock solution of 10^8 CFU/mL log-phase BCG cell suspension [based on optical density (A_{600}) measurements] in 7H9 was split into three 10 mL BCG cultures for control, RIF-treated, and INH-treated cells. Antibiotic concentration was 1 μg/mL for both drugs. BCG were cultured in Difco Middlebrook 7H9 Broth (BD Diagnostics, Sparks, MD) supplemented with 10% (v/v) ADC enrichment and 0.05% Tween 20. The cells were cultivated in a shaker at 37°C for 4 days.

4.3.3 Cell preparation

1 mL samples were extracted on the initial day and 4th day after drug insertion. Initial tests diluted the suspension 10% ($\sigma_m = 0.07$ S m^{-1}) in deionized water (DI). Heat-treatment of cells was conducted by submerging the vials in a heated water bath for 10 minutes. To obtain heat-killed cells, 500 μL of control cells were exposed to a higher temperature of 85ºC for a longer time of 30 minutes. Later tests involving different conductivities of medium used 20%,

30%, 40%, and 50% dilution with DI water ($\sigma_m = 0.11, 0.16, 0.21, \text{and } 0.26\ \text{S m}^{-1}$, respectively). The medium conductivity was measured using a conductivity meter (Thermo Scientific, MA). The prepared cells were stained with Live/Dead *Bac*light kit (Invitrogen, Carlsgad, CA) for labeling. The stained cells were incubated at room temperature for 15 minutes prior to experimentation.

4.3.4. Scanning electron microscopy

To prepare for SEM imaging, 5 μL of cells from each culture were dropped onto piranha-cleaned silicon chips. The chip was left to dry in a biosafety hood for 1 hour. Once dried, the chips were washed by slowly dipping into DI water then carefully blow dried using N_2 gas. This was repeated three times until no residue was left on the surface. When placed in the SEM, the stages were tilted 30 degrees to observe the perturbation of the surface.

4.3.5 Experimental setup

A planar gold electrode with a gap length of 10 μm was used to characterize the electrokinetic responses of BCG cells. The electrodes were connected to a function generator (Agilent 33220A, Santa Clara, CA) with a frequency ranging from 1 kHz to 10 MHz for 1 minute. The applied voltage was 20 $V_{p.p.}$, except for frequencies of 1 kHz and 10 kHz where 6 $V_{p.p.}$ and 12 $V_{p.p.}$ were used, respectively. At the lower frequencies, the voltages needed to be reduced to prevent electrical breakdown in the solution. A fluorescent microscope (Nikon Eclipse 55i) recorded and imaged the cells after 1 minute. A depiction of the setup is shown in Figure 4.4.b.

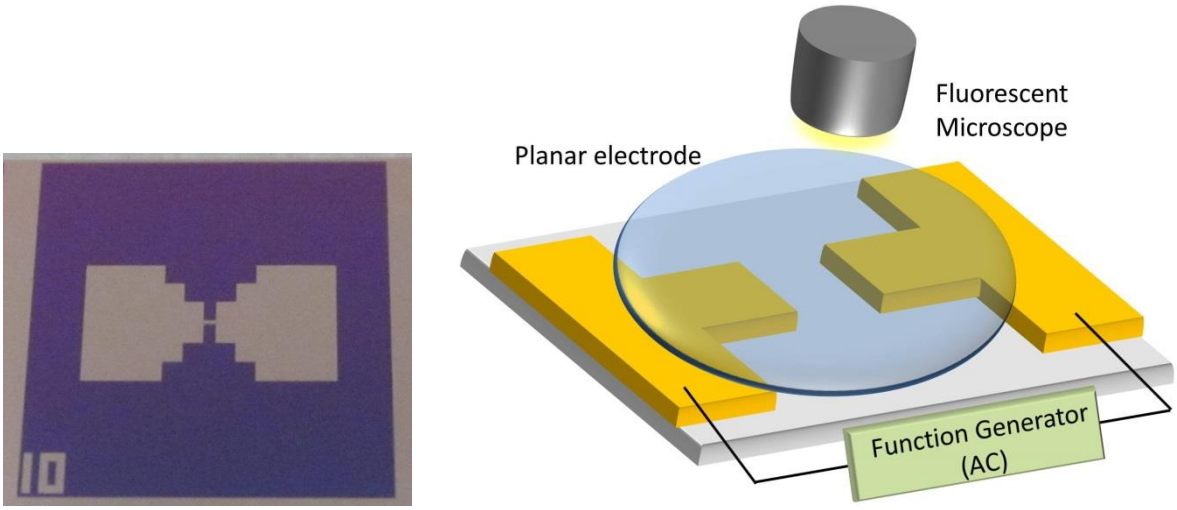

(a) (b)

Figure 4.4. (a) Fabricated planar electrodes with a gap size of 10 μm. (b) Illustration of the experimental setup.

To determine the crossover frequency and crossover medium conductivity, the same set-up was used but the applied frequencies were changed. Frequency was slowly increased to 0.1, 0.2, 0.4, 0.6, 0.8, 1, 2, 4, 5, 6, 8, 10, 20 MHz with 10 second intervals. Frequency was then decreased in the reverse order to determine when cells detached from electrode edge. This was repeated for all medium conductivity tested. The same Nikon microscope was used to record and image the cells.

3.3.5 Numerical computation

The properties of cells were estimated by sampling analysis with COMSOL Multiphysics. A range of variables were selected, and the sampling analysis determined the values of the parameter variables to fit the experimental results. Note that the numerical simulation was completed in collaboration with Hyun-Boo Lee.

4.4 Results and Discussion

4.4.1 Temperature effect on DEP

The effect of temperature on electrokinetic responses has extensively been studied on yeast and other cells [126] but not *Mycobacterium* cells. Lethal temperatures have often been used to obtain "heat treated" or "boiled" cells to model non-viable cells in hopes of studying the differences in the electrokinetic behavior of live and dead cells [121, 127, 128]. Since these tests have not been conducted for *Mycobacterium*, the effects for various temperatures were evaluated.

Control cells treated at various temperatures from 50ºC to 80ºC for 10 minutes were investigated on an isolated planar electrode to determine changes to BCG cells electrophysiology and its response to DEP. Using the previously determined optimal frequency of 5 MHz, the number of the cells attracted to the electrode in the fixed timeframe were found to decrease as the temperature increased. This is shown in Fig. 4.5 by counting the immobilized cells. The DEP response of BCG cells was similar to the control up to 60ºC. Over 60ºC, the number of attracted cells was reduced by half.

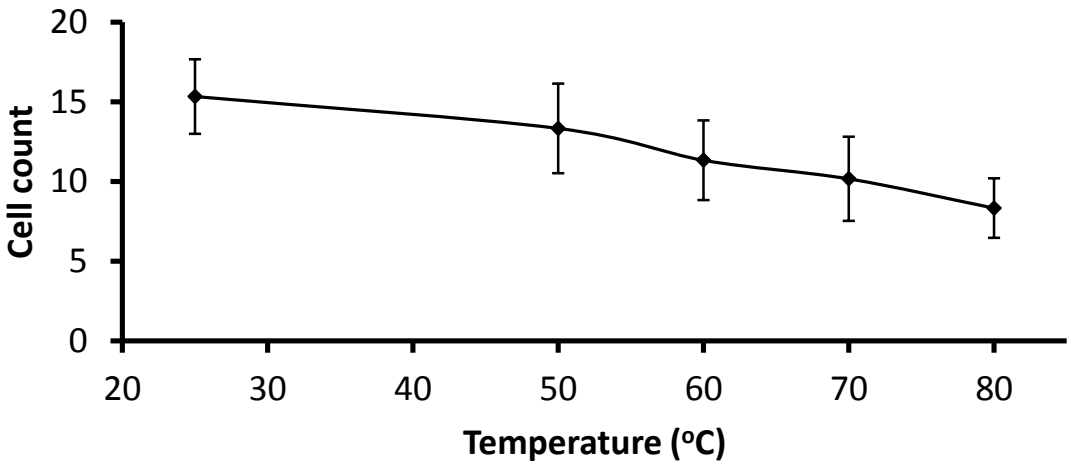

Figure 4.5. Cell count of BCG cells attracted to planar electrode edge after treatment at varying temperatures.

The temperature results correlated well with the previous assumption of a phase-shift of the cell wall at 60ºC [64]. Prior to the phase-shift temperature, the *Mycobacterium* cell wall and membrane remained intact and retained its low conductivity. Once the temperature became higher than the phase-shift temperature of 60ºC, there was an increase in the permeability of the cell. This might alter the conductivity and permittivity of the cell membrane and wall, therefore, a noticeable change in DEP at the higher temperatures. Previous work by Doig and colleagues suggest 10 minutes may not be enough. They reported that heating to 80°C for 20 minutes fully submerged in a water bath may be needed to kill all BCG cells [77]. Therefore, BCG cells were submerged in 85°C for 30 minutes to determine the first crossover frequency of heat-killed cells.

SEM images of the different heat-treated cells were taken to observe the morphological changes (Fig 4.6). In Fig 4.6. a and b, SEM shows that 60°C treated cells were similar to control cells in the shapes, perhaps with very small perturbations on the surface. Fig 4.6.c of 80°C treated cells confirms visible changes to the surface. The biggest change was seen with heat-

killed cells (Fig 4.6.d). Some cells looked flat, most likely due to the cytoplasm escaping the ruptured cells. Others were swollen with a visible depreciated ring around them. The swelling may be due to osmosis, causing medium solution to permeate through the barely intact cell structure. The higher magnification of the heat-killed cells (Fig 4.6.f) shows the depreciated ring to be around 60 nm. Cryo-electron images have illustrated *Mycobacterium* consists of a cell wall structure with a thickness of ~50 nm and membrane with a thickness ~10 nm [129]. These results suggest heat-killing of cells will greatly affect (1) wall and membrane structure and thus the specific capacitance of the outer shell structure, and (2) cytoplasm conductivity.

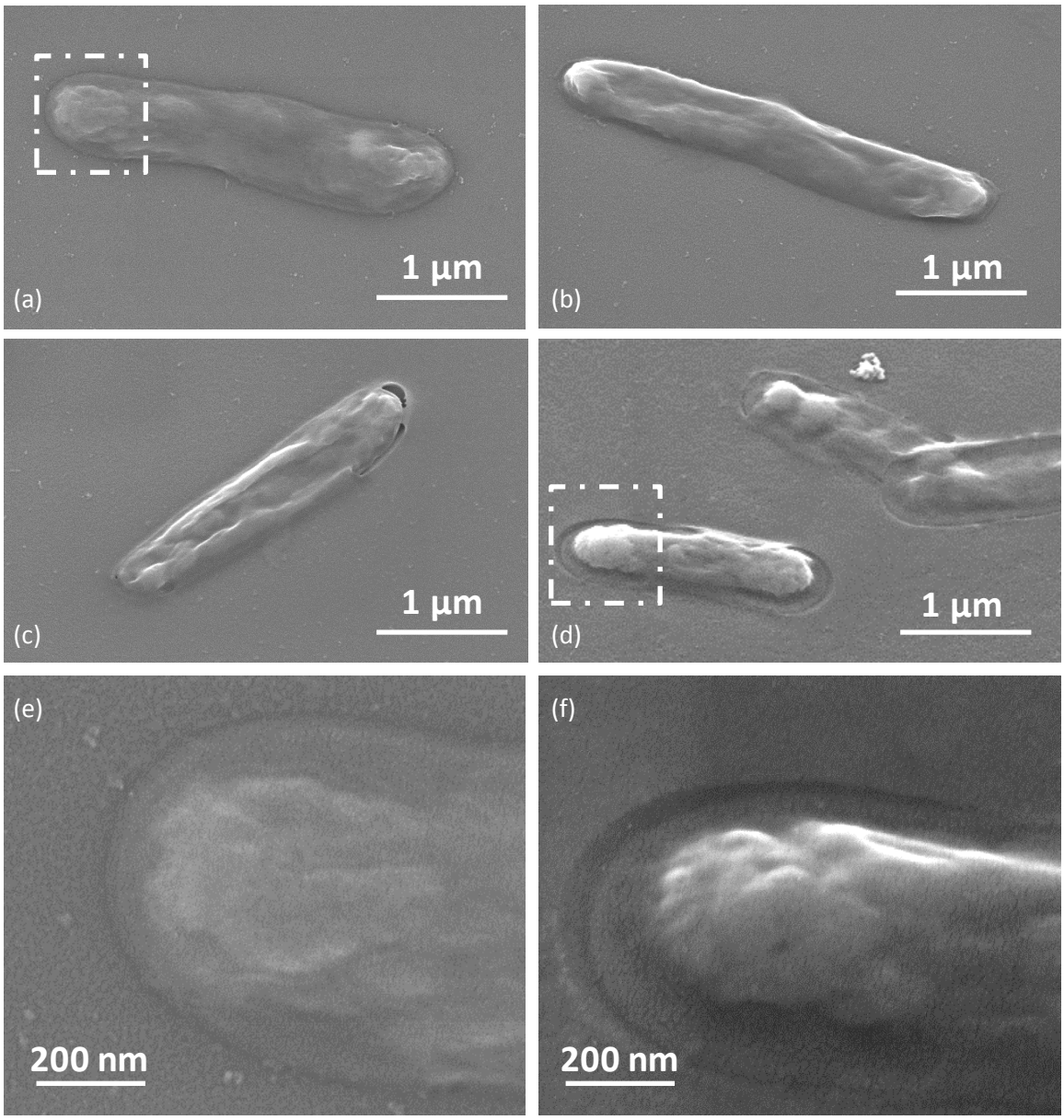

Figure 4.6. SEM images of BCG cells treated with different temperatures. a) Not heat-treated control cells. Heat-treated for 10 minutes at b) 60°C and c) 80°C. d) Heat-killed cells treated for 30 minutes at 85°C. Higher magnification image of boxed areas from e) control and f) heat-killed cells illustrates the morphological changes to the cell envelope and cytoplasm.

4.4.2 Diffentiation of control and heat-killed BCG cells

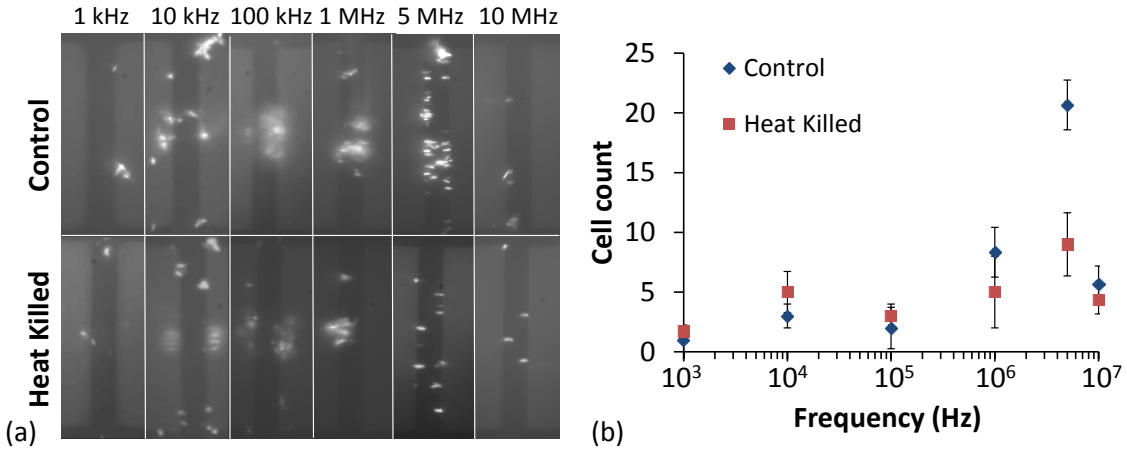

Figure 4.7. Comparison of heat-killed and control cells at frequencies ranging from 1 kHz to 10 MHz. a) Image of planar electrode gap after applying said frequency for 1 minute. b) Count of immobilized cells attracted to electrode edge.

Electrokinetic responses of control and heat-killed BCG cells for various frequencies were investigated using the previously studied experimental setup. The results are shown in Fig. 4.7. Each cell suspension of 2 μL was exposed to frequencies ranging from 1 kHz to 10 MHz on a planar electrode for 1 minute. Interaction between DEP and ACEO was found to be the same for control and heat-killed BCG cells. For the frequency of 1 kHz and 10 MHz, the motion of the cells was small due to the limitations of ACEO; however, the attracted cells were immobilized on the edges of the electrode for 10 MHz showing positive DEP. Most BCG cells moved at frequencies ranging from 10 kHz to 5 MHz. At 10 and 100 kHz, the attracted cells accumulated near the center of the electrode forming vortices and were dominated by ACEO fluid flow. 1 MHz showed attraction of cells close to the surfaces, where some cells could be seen sliding on the edges of the electrode. This shows that positive DEP and ACEO forces were comparable. The most noticeable difference came at 5 MHz, where cells were still immobilized on the edges like control cells; however, unlike the control cells, the number of immobilized cells was far less

for the heat-killed cells (Fig. 4.6.b). The damaged BCG cells had a much weaker DEP force than the intact control cells; therefore, could be differentiated from control cells.

Since ACEO is a function of medium conductivity and frequency and not the particle properties, the difference detected at 5 MHz comes from DEP's sensitivity to the altered properties of heat-killed BCG cells. The first crossover frequency can be used estimate the cell properties (Eqn. 4.1); however, the crossover frequency for heat-killed cells was 1 MHz, same as the control cells. Relying purely on this crossover frequency would show cell properties similar to control cells, which is incorrect according to the result from 5 MHz. To obtain a better estimation of the properties, the crossover frequency at different medium conductivities must be investigated.

4.4.3 Characterization of control and heat-killed BCG cells

Crossover frequencies of control and heat-killed BCG cells were evaluated with varying medium conductivities ($\sigma_m = 0.07, 0.11, 0.16, 0.21, \text{and } 0.26\ \text{S m}^{-1}$) and shown in Fig 4.8. Heat-killing the cells showed an overall shift of the crossover frequency to the left. Sensitivity study on the crossover frequency showing a leftward shift in the linear region (1 ~ 5 MHz) is from the reduction in the permittivity of the cell wall and membrane. A shift to the left in the non-linear region (10 ~ 20 MHz) is from the reduction of the cytoplasm conductivity.

The experimental data was fitted with numerical double-shell ellipsoid model using sampling analysis via COMSOL Multiphysics. A range of parameter values were determined for each dielectric variable to evaluate combinations that fit the crossover frequency profile at different medium conductivities. The estimations of the BCG cells are shown in Table 4.1. The permittivity of the wall and membrane were changed to specific capacitance so that it could be

combined by assuming an electrical model of the layers as serially connected capacitors. By doing so, we can evaluate the effective specific capacitance of the outer shell structure (C_{shell}) to compare before and after being rendered non-viable. The reasoning for this transformation is because the values of membrane and wall permittivity had high variability, where the sampling analysis showed decreasing one permittivity value could be compensated by increasing the other. Converting them into an effective capacitance, however, showed high correlation and low deviations among the sampling method. The results will give a more accurate representation of the effect of the treatment process on the outer structure.

Table 4.1. Estimation of control and heat-killed BCG cell properties extracted from crossover frequencies at various medium conductivities.

Sample	ε_{wall}	ε_{mem}	$C_{shell}\left(\frac{mF}{m^2}\right)$	$\sigma_{cyto}\left(\frac{S}{m}\right)$
Control	32	8.6	2.87	0.58
Heat-killed	10.5	9.9	1.48	0.41

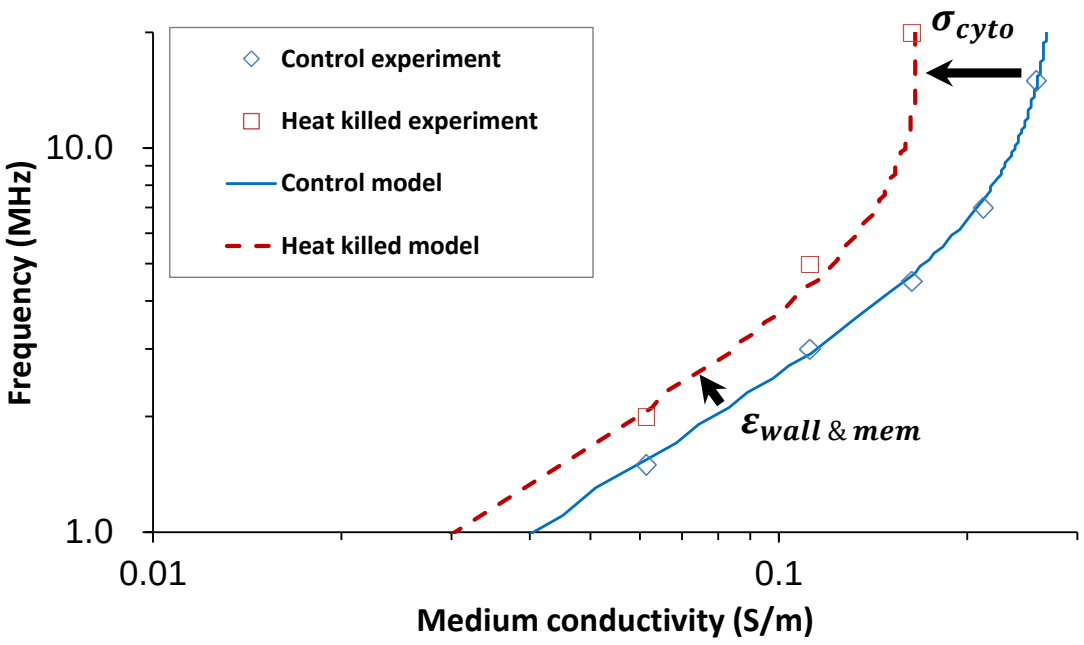

Figure 4.8. Crossover frequency of control and heat-killed BCG cells. The shift to the left after lethal temperatures arises from the decrease in permittivity of the outer structure (wall and membrane) and cytoplasm conductivity.

The first crossover frequency, f_{x1}, is highly sensitive to the permittivity of the cell membrane and wall. Comparing C_{shell} shows a 48% reduction in capacitance after heat-killing. This large change can be seen with the leftward shift in the linear region (1 ~ 5 MHz) in Fig 4.8. SEM images of the cell envelope (Fig 4.6.e,f) showed the cell wall and membrane structure to be completely different after being heat-killed. The depreciated ring around the cells is consistent with *Mycobacterium* cell wall and membrane thickness (50-70 nm), meaning the cell envelope may have lost its structural integrity after lethal temperatures and could not retain its shape in the vacuum chamber when observed under SEM.

The second crossover frequency, f_{x2}, is mostly dependent on the cytoplasm conductivity. Although the experiments here did not test for f_{x2} at the higher frequency of ~100 MHz, σ_{cyto}

can be evaluated by the shift of the crossover frequency at frequencies of 10~20 MHz. Heat-killing showed a reduction of 29% in cytoplasm conductivity. The conductivity of a cell's interior can be as high due to the many ions and charged particles stored in the cytoplasm. Once the envelope became more permeable, water might have flowed into the cell which would reduce the conductivity. This notion is supported with the SEM image showing bloated BCG cells. At the same time, the cell could have lysed, which would result in the cytoplasm escaping the cells. SEM images also captured images of nearly empty BCG cells, which support this idea.

4.4.4 Drug effect on DEP

DEP has been used as a rapid antibiotic susceptibility tool for various types of drugs and cells. Cells such as human myelogenous leukemia cells [123], *Staphylococcus epidermidis* [124], and *E.coli* [83] have been tested. Drugs that altered the specific capacitance of the membrane were observed to affect the DEP response. Hawkins *et al.* have found similar results when characterizing *Mycobacterium smegmatis*, a fast growing family of *Mycobacterium*, with treatment of ethambutol [82]. Ethambutol is a drug that inhibits the production of arabinogalactan and thus the mycolic acids in the cell wall. The removal of a major component of the cell wall caused significant decrease in the effective permittivity of the cell, which resulted in detectable changes by DEP.

M. tuberculosis, however, is a very slow growing bacterium unlike *M. smegmatis. M. bovis* BCG is a *Mycobacterium tuberculosis* complex cell which causes tuberculosis in cows and cultures very similarly to *M. tuberculosis*, thus should give a better representation of *M. tuberculosis*.

For *M. tuberculosis*, there are two main drugs to consider. MDR-TB is defined as TB resistant to one of the first-line drugs rifampin (RIF) or isoniazid (INH). Both RIF and INH are considered to be the most important antituberculosis drugs. The investigation of the DEP behavior of the cells treated with these drugs is therefore very important. Interestingly, RIF and INH have completely different mechanism to kill *Mycobacterium* cells and may affect DEP differently.

One of the main reasons for treatment failure is from resistance to RIF [130, 131]. RIF resistant strains occur most often in strains that are also resistant to INH, making RIF a great surrogate maker for MDR-TB [132]. The mechanism of action of RIF is the inhibition of mycobacterial transcription by targeting DNA-dependent β-subunit of RNA polymerase [133, 134]. RIF permeates through the cell structure to bind with the RNA polymerase to kill the cell. 96% of resistances to RIF are due to a mutation in the well-defined 81-bp region of *rpoB*. This makes genotypic methods effective when detecting for RIF-resistance and MDR-TB.

INH is one of the most efficient drugs for treating TB even after 50 years. It is a potent prodrug which enters the cell through passive diffusion [135] and activated by mycobacterial enzyme *katG* [36]. INH inhibits the synthesis of mycolic acids in the *Mycobacterium* cell wall structure by disrupting the enzyme involved in the mycolic acid biosynthesis [136, 137]. This ultimately leads to cell death. It has been reported that INH induces morphological changes in mycobacteria, such as loss of structure or appearance of surface wrinkles and bulging [138, 139]. Because of the alterations to the cell wall, the DEP characteristic of INH-treated cells should be very different from control and RIF-treated BCG cells.

To correlate the DEP response with the mechanism of action of the drugs, BCG cells cultured for 4 days in media with RIF and INH were imaged with SEM. The SEM images showed morphological changes for INH but minimal changes for RIF (Fig 4.9). In Fig 4.9. a and c, RIF-treated cells have very smooth surfaces with some blebing like structure. However, the cells overall looked very similar to control and 60℃ treated cells. The INH-treated cells, on the other hand, were very swollen with surface deformations and had a ring formation around the cells (Fig. 4.9. b and d). These rings were consistent with the previous findings from heat-killed cells, where the distance matched the thickness of cell wall and membrane [129]. Previous research has shown that heat-treatment can have similar effects to INH, where heat-treatment of *M. smegmatis* inactivated the temperature-sensitive *inhA* gene, which had a similar effect to INH treatment (morphological changes, cell lysis, inhibition of mycolic acid synthesis, and accumulation of long fatty chains) [140].

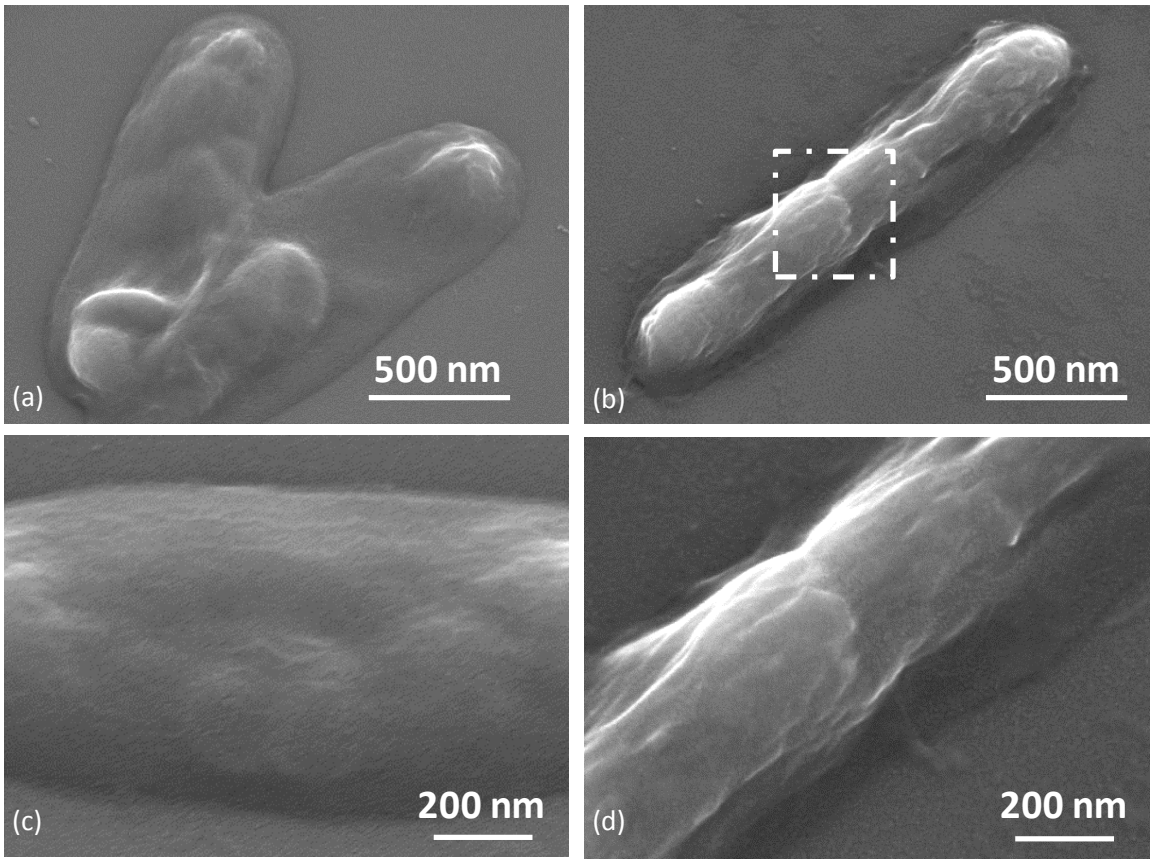

Figure 4.9. SEM images of RIF and INH-treated BCG cells after 4 days of culture. a, c) RIF cells showing minimal changes to the morphology. b, d) INH-treated cell showing large changes to the surface and cytoplasm.

4.4.5 Characterization of control and drug-treated BCG cells

4 day drug-treated BCG cells were characterized by measuring the altered crossover frequency at various medium conductivities (Fig 4.10). The evaluated medium conductivities were the same as the heat-killed experiments. The experimental data was again fitted with numerical double-shell ellipsoid model using sampling analysis via COMSOL Multiphysics. The computed properties are shown in Table 4.2.

Fig 4.10 shows that the crossover frequency of INH-treated cells was greatly affected compared to RIF-treated cells. This large shift for INH equates to a massive reduction in the permittivity of the membrane and wall parameters. The computed specific capacitance of the cell envelope showed a reduction of 78%. This result is consistent with the INH mechanism of action, where inhibition of the mycolic acid in the cell wall greatly affects the effective capacitance of the cell, producing a very noticeable effect on DEP. SEM images of INH-treated cells (Fig 4.9, b and d) shows the damages to the cell structure.

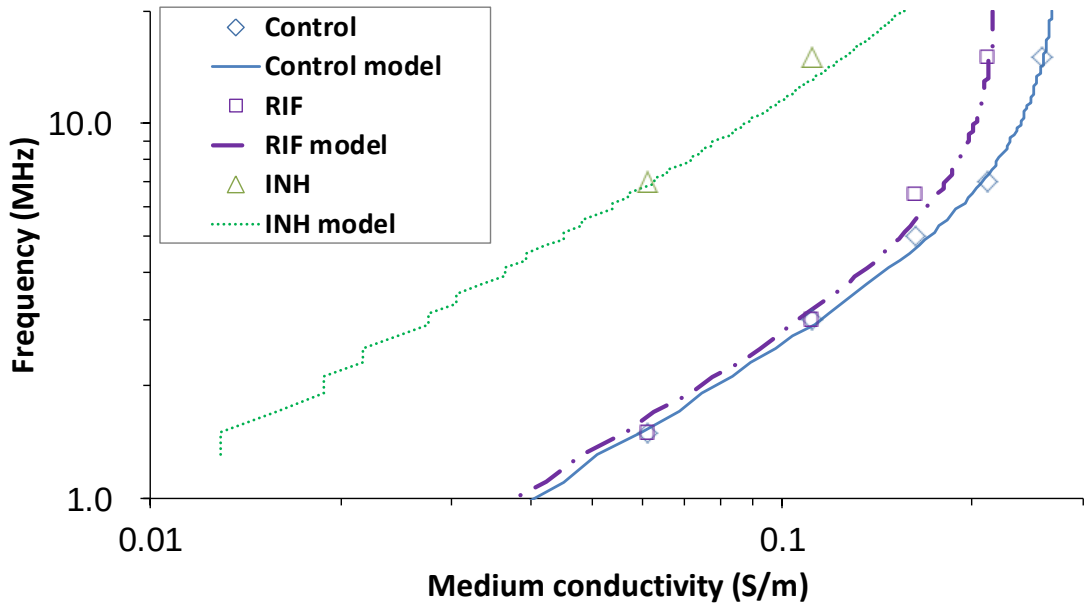

Figure 4.10. Crossover frequency of control and drug-treated BCG cells after 4 days. The large shift of INH-treated cells arises from the decrease in permittivity of the outer structure (wall and membrane) and cytoplasm conductivity. Cof of RIF-treated cells shows permittivity of the envelope remained the same but there was a slight decrease in the cytoplasm conductivity.

Table 4.2. Estimation of control and drug-treated BCG cell properties extracted from crossover frequencies at various medium conductivities.

Sample	ε_{wall}	ε_{mem}	$C_{shell}\left(\frac{mF}{m^2}\right)$	$\sigma_{cyto}\left(\frac{S}{m}\right)$
Control	32	8.6	2.87	0.58
RIF	28.2	6.4	2.21	0.47
INH	7.8	6.9	0.628	0.51

RIF-treated cells, on the other hand, shows very little effect on the permittivity of the cell envelope. The crossover frequency was similar with control up to 10 MHz where conductivity of the cytoplasm comes into effect. Computed properties showed a reduction of 19% of the cytoplasm conductivity for RIF-treated cells. This reduction could come from the cell ceasing to function, reducing the amount of ions and charged particles produced in the cytoplasm. SEM images also showed consistent results (Fig. 4.9, a and c), where the surface was very smooth without formation of a depreciated ring unlike INH-treated and heat-killed cells.

4.4.5 Differentiation of control and drug-treated BCG cells

BCG cells incubated in medium with RIF and INH were attempted to be differentiated using the planar electrode on different days by counting the number of cells immobilized at the optimized frequency of 5 MHz after 1 minute. The results are shown in Fig 4.11. DEP was similar for all the cells for the first 24 hours (1st day). On the 2nd day, the INH-treated cells were slightly less attracted compared to RIF and control cells; however, the error-bars were overlapped thus was not statistically significant. INH-treated cells were able to be differentiated from control on the 4th day but RIF-treated cells could not. These results are consistent with the

hypothesis that INH treatment greatly affects the cell envelope and the capacitance of the cell, therefore causing a noticeable effect on DEP while RIF has a minimal effect.

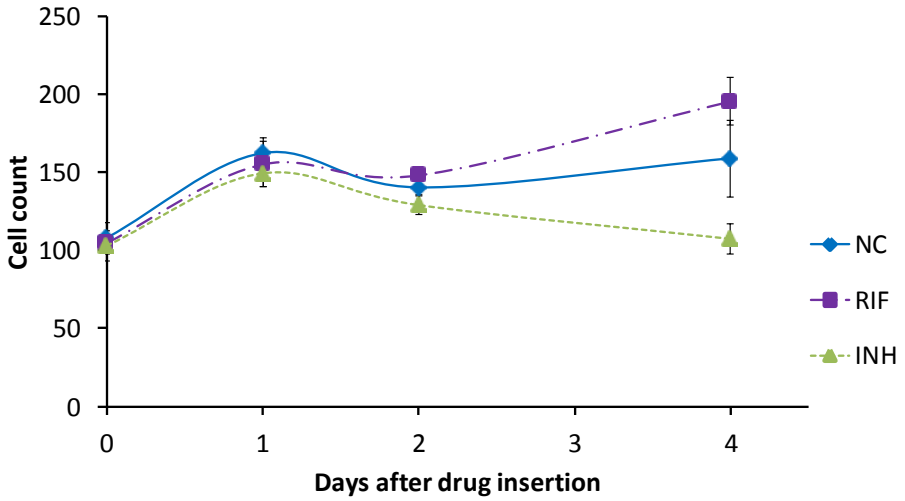

Figure 4.11. Cell count of immobilized BCG cells on planar electrode on different days after drug insertion into culture media. 4th day shows a noticeable difference between INH and control, but not RIF-treated cells.

After characterization of RIF-treated cells, it was expected that RIF will demonstrate similar DEP response as control and may not be able to be differentiated unless a higher medium conductivity and frequency is used. However, doing so resulted in a reduction in AC electroosmosis, which will reduce the amount of cells brought to the electrode gap, thereby reducing the sensitivity and increasing the detection time of the sensor. Since the goal is to develop a rapid and sensitive drug-susceptibility test, the higher frequency and medium conductivity cannot be implemented into the current system.

To differentiate RIF-treated cells from control, the intensity of the captured cells was measured. *Mycobacterium* is known for the waxy walls [141], which causes dividing cells to become easily clumped together. Clumping of cells was observed to increase the fluorescence signal. Thus, viable and clumpy BCG cells were observed to be brighter under fluorescence when captured than individually captured RIF-treated cells as seen in Fig. 4.12.a. The intensity of the region of interest was normalized by dividing by the background intensity. This measurement yielded in differentiation of RIF-treated cells by the 2nd day (Fig 4.12.b).

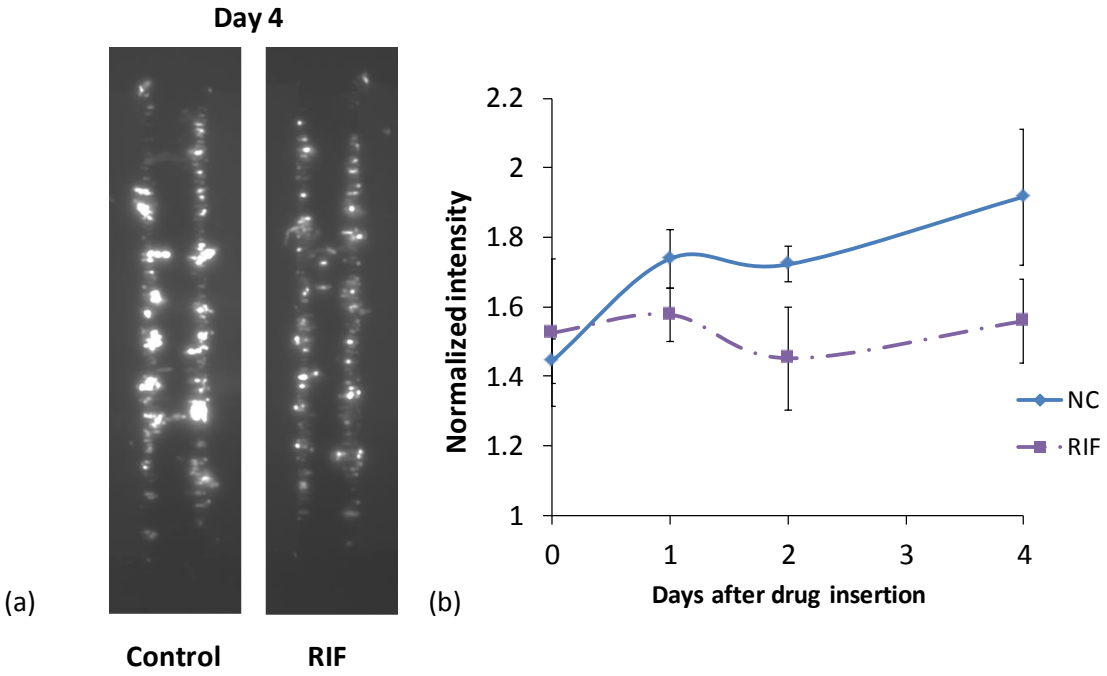

Figure 4.12. Normalized intensity of control and RIF-treated BCG cells over a 4 day period. a) Image of BCG cells captured on 4th day. b) Normalized intensity over 4 days.

4.5 Summary

In this chapter, we have demonstrated rapid differentiation and characterization of *M. bovis* BCG using dielectrophoresis after being rendered non-viable through heat-killing and drug treatment of rifampin and isoniazid. This represents the first case of dielectrophoresis characterization method for non-viable BCG cells. Dielectrophoresis measurements show that both heat-killing and isoniazid make a significant effect on the capacitance of the cell envelope, which is consistent with the drug mechanism of INH inhibiting synthesis of the cell wall structure and temperature affecting the cell envelope. These cells were readily differentiated from control; however, rifampin could not be differentiated due to the drug not affecting the specific capacitance of the cell envelope. Rifampin-treated cells were only differentiated by employing the intensity measurements. The results are summarized in Table 4.3.

The results indicate that electrokinetic forces of ACEO and DEP can be exploited to evaluate for drug-susceptibility of *Mycobacterium tuberculosis* complex cells. This platform can be transferred to microfluidic or microtip devices to be further developed into rapid biosensors.

Table 4.3. Relating heat-killing and drug mechanism of action with respect to dielectrophoretic response of *M. bovis* BCG cells.

Rendering non-viable	Mechanism of action	Cell envelope affected	DEP differentiation from control
Heat-killed	• **Cell wall becomes more permeable** • **SEM shows depreciated ring around cells**	**YES**	**Cell counting**
INH	• **Inhibit synthesis of mycolic acid in cell wall** • **SEM shows depreciated ring around cells**	**YES**	**Cell counting**
RIF	• **Inhibits RNA transcription** • **SEM shows cells similar to control**	**NO**	**Intensity measurement**

Chapter 5: Summary and Future Work

Drug-susceptibility tests are lacking in detection of multi-drug resistant tuberculosis. Current phenotypic drug-susceptibility methods may take days to weeks to detect rifampin and isoniazid susceptibility [32, 33]. Faster genotypic methods can be limited by cost and non-gene specific resistances. To address this need, we have developed a microtip immunosensor to detect *Mycobacterium* from sputum samples using electrokinetic forces. The detection time was 30 minutes with a detection limit was 100 CFU/mL. However, dielectrophoresis has never been used to test for drug-susceptibility of *Mycobacterium tuberculosis* complex cells and needed to be investigated.

To address this, a fundamental study on the electrokinetic forces of dielectrophoresis and AC electroosmosis was conducted on *Mycobacterium tuberculosis* complex cells. An optimal frequency and medium conductivity which balanced the electrokinetic forces was found at 5 MHz and 0.07 S m^{-1}. The temperature effect on *M. bovis* BCG cells were characterized and differentiated to model non-viable cells. Finally, two significant drugs in treatment of TB, rifampin and isoniazid, were investigated on their effect on dielectrophoresis and the altered dielectric properties characterized. Treatments which rendered cells non-viable by affecting the cell envelope, such as lethal temperature and isoniazid, significantly affected the dielectrophoretic response by altering the capacitance of the cell. Rifampin, which did not affect the cell envelope and thus the capacitance, was differentiated by measuring the intensity difference between clumpy, viable BCG cells and individual cells.

Future research will focus on the further development of a drug-susceptibility sensor. Electrokinetic based detection showed detection as fast as 4 days, possibly even sooner with further optimization. The science and technology gained from this study will be transitioned onto microtip- and nanotip sensors. By doing so, a rapid and sensitive yet inexpensive drug-susceptibility test can be developed.

List of References

1. WHO. *Tuberculosis*. Fact sheet N°104 2012.
2. WHO, *Global Tuberculosis Control: WHO Report*. 2011, WHO: Geneva, Switzerland.
3. Caws, M. and F.A. Drobniewski, *Molecular techniques in the diagnosis of Mycobacterium tuberculosis and the detection of drug resistance.* New Vistas in Therapeutics, from Drug Design to Gene Therapy: Drug-Resistant Tuberculosis, from Molecules to Macro-Economics, 2001. **953**: p. 138-145.
4. Cardona, M., et al., *Transmission of tuberculosis from a seven-year-old child in a Sydney school.* Journal of Paediatrics and Child Health, 1999. **35**(4): p. 375-378.
5. Rajagopalan, S., *Tuberculosis and aging: A global health problem.* Clinical Infectious Diseases, 2001. **33**(7): p. 1034-1039.
6. Steingart, K.R., A. Ramsay, and M. Pai, *Optimizing sputum smear microscopy for the diagnosis of pulmonary tuberculosis.* Expert Review of Anti-Infective Therapy, 2007. **5**(3): p. 327-331.
7. Chin, D.P., et al., *Spread of Mycobacterium tuberculosis in a community implementing recommended elements of tuberculosis control.* Jama-Journal of the American Medical Association, 2000. **283**(22): p. 2968-2974.
8. WHO, *Towards universal access to diagnosis and treatment of multidrug-resistant and extensively drug-resistant tuberculosis by 2015*, in *WHO Progress Report*. 2011: Geneva, Switzerland.
9. Cohn, D.L., F. Bustreo, and M.C. Raviglione, *Drug-resistant tuberculosis: Review of the worldwide situation and the WHO/IUATLD global surveillance project.* Clinical Infectious Diseases, 1997. **24**: p. S121-S130.
10. WHO, *Multidrug and extensively drug-resistant TB (M/XDR-TB): 2010 global report on surveillance and response*, in *WHO Global Report*. 2010: Geneva, Switzerland. p. 71.
11. WHO, *Molecular line probe assays for rapid screening of patients at risk of multi-drug resistant tuberculosis (MDR-TB)*, in *Expert Group Report*. 2008: Geneva, Switzerland.
12. Corbett, E.L., et al., *The growing burden of tuberculosis - Global trends and interactions with the HIV epidemic.* Archives of Internal Medicine, 2003. **163**(9): p. 1009-1021.

13. Dye, C., et al., *Evolution of tuberculosis control and prospects for reducing tuberculosis incidence, prevalence, and deaths globally.* Jama-Journal of the American Medical Association, 2005. **293**(22): p. 2767-2775.
14. Steingart, K., et al., *Fluorescence versus conventional sputum smear microscopy for tuberculosis: a systematic review.* Lancet Infectious Diseases, 2006. **6**(9): p. 570-581.
15. Drobniewski, F., et al., *Diagnosis of tuberculosis and drug resistance: what can new tools bring us?* International Journal of Tuberculosis and Lung Disease, 2012. **16**(7): p. 860-870.
16. Steingart, K.R., et al., *Sputum processing methods to improve the sensitivity of smear microscopy for tuberculosis: a systematic review.* Lancet Infectious Diseases, 2006. **6**(10): p. 664-674.
17. Davis, J.L., et al., *Diagnostic accuracy of same-day microscopy versus standard microscopy for pulmonary tuberculosis: a systematic review and meta-analysis.* Lancet Infectious Diseases, 2013. **13**(2): p. 147-154.
18. Cattamanchi, A., et al., *Does Bleach Processing Increase the Accuracy of Sputum Smear Microscopy for Diagnosing Pulmonary Tuberculosis?* Journal of Clinical Microbiology, 2010. **48**(7): p. 2433-2439.
19. Bonnet, M., et al., *Bleach sedimentation: An opportunity to optimize smear microscopy for tuberculosis diagnosis in settings of high prevalence of HIV.* Clinical Infectious Diseases, 2008. **46**(11): p. 1710-1716.
20. Gandhi, M.P., et al., *Sputum Smear Microscopy at Two Months into Continuation-Phase: Should It Be Done in All Patients with Sputum Smear-Positive Tuberculosis?* Plos One, 2012. **7**(6).
21. Seung, K.J., *Does My Patient Have Multidrug-Resistant Tuberculosis?* Clinical Infectious Diseases, 2010. **51**(4): p. 379-380.
22. Heifets, L.B. and R.C. Good, *Current laboratory methods for the diagnosis of tuberculosis.* 1994.
23. Chew, W.K., et al., *Clinical evaluation of the Mycobacteria growth indicator tube (MGIT) compared with radiometric (Bactec) and solid media for isolation of Mycobacterium species.* Journal of Medical Microbiology, 1998. **47**(9): p. 821-827.

24. Hanna, B.A., et al., *Multicenter evaluation of the BACTEC MGIT 960 system for recovery of mycobacteria.* Journal of Clinical Microbiology, 1999. **37**(3): p. 748-752.
25. Benjamin, W.H., et al., *Comparison of the MB/BacT system with a revised antibiotic supplement kit to the BACTEC 460 system for detection of mycobacteria in clinical specimens.* Journal of Clinical Microbiology, 1998. **36**(11): p. 3234-3238.
26. Drobniewski, F.A., et al., *Modern laboratory diagnosis of tuberculosis.* The Lancet Infectious Diseases, 2003. **3**(3): p. 141-147.
27. Moore, D.A.J. and N.S. Shah, *Alternative Methods of Diagnosing Drug Resistance-What Can They Do for Me?* Journal of Infectious Diseases, 2011. **204**: p. S1110-S1119.
28. Caviedes, L., et al., *Rapid, efficient detection and drug susceptibility testing of Mycobacterium tuberculosis in sputum by microscopic observation of broth cultures.* Journal of Clinical Microbiology, 2000. **38**(3): p. 1203-1208.
29. WHO *Noncommercial culture and drug-susceptibility testing methods for screening patients at risk for multidrug-resistant tuberculosis*. 2011.
30. Minion, J., et al., *Microscopic-observation drug susceptibility and thin layer agar assays for the detection of drug resistant tuberculosis: a systematic review and meta-analysis.* Lancet Infectious Diseases, 2010. **10**(10): p. 688-698.
31. Martin, A., et al., *The nitrate reductase assay for the rapid detection of isoniazid and rifampicin resistance in Mycobacterium tuberculosis: a systematic review and meta-analysis.* Journal of Antimicrobial Chemotherapy, 2008. **62**(1): p. 56-64.
32. Bwanga, F., et al., *Direct susceptibility testing for multi drug resistant tuberculosis: A meta-analysis.* Bmc Infectious Diseases, 2009. **9**.
33. Bwanga, F., et al., *Direct Nitrate Reductase Assay versus Microscopic Observation Drug Susceptibility Test for Rapid Detection of MDR-TB in Uganda.* Plos One, 2011. **6**(5).
34. Abebe, G., et al., *Tuberculosis drug resistance testing by molecular methods: Opportunities and challenges in resource limited settings.* Journal of Microbiological Methods, 2011. **84**(2): p. 155-160.
35. Drobniewski, F.A. and S.M. Wilson, *The rapid diagnosis of isoniazid and rifampicin resistance in Mycobacterium tuberculosis - a molecular story.* Journal of Medical Microbiology, 1998. **47**(3): p. 189-196.

36. Zhang, Y., et al., *The Catalase Peroxidase Gene and Isoniazid Resistance of Mycobacterium-Tuberculosis.* Nature, 1992. **358**(6387): p. 591-593.
37. Telenti, A., et al., *Genotypic assessment of isoniazid and rifampin resistance in Mycobacterium tuberculosis: A blind study at reference laboratory level.* Journal of Clinical Microbiology, 1997. **35**(3): p. 719-723.
38. Huang, W.L., et al., *Performance Assessment of the GenoType MTBDRsl Test and DNA Sequencing for Detection of Second-Line and Ethambutol Drug Resistance among Patients Infected with Multidrug-Resistant Mycobacterium tuberculosis.* Journal of Clinical Microbiology, 2011. **49**(7): p. 2502-2508.
39. Ando, H., et al., *Evaluation of a line probe assay for the rapid detection of gyrA mutations associated with fluoroquinolone resistance in multidrug-resistant Mycobacterium tuberculosis.* Journal of Medical Microbiology, 2011. **60**(2): p. 184-188.
40. Acuna-Villaorduna, C., et al., *Cost-effectiveness analysis of introduction of rapid, alternative methods to identify multidrug-resistant tuberculosis in middle-income countries.* Clinical Infectious Diseases, 2008. **47**(4): p. 487-495.
41. Morgan, M., et al., *A commercial line probe assay for the rapid detection of rifampicin resistance in Mycobacterium tuberculosis: a systematic review and meta-analysis.* Bmc Infectious Diseases, 2005. **5**.
42. Saribas, Z., et al., *Use of fluorescence resonance energy transfer for rapid detection of isoniazid resistance in Mycobacterium tuberculosis clinical isolates.* International Journal of Tuberculosis and Lung Disease, 2005. **9**(2): p. 181-187.
43. Varma-Basil, M., et al., *Rapid detection of rifampin resistance in Mycobacterium tuberculosis isolates from India and Mexico by a molecular beacon assay.* Journal of Clinical Microbiology, 2004. **42**(12): p. 5512-5516.
44. Edwards, K.J., et al., *Detection of rpoB mutations in Mycobacterium tuberculosis by biprobe analysis.* Journal of Clinical Microbiology, 2001. **39**(9): p. 3350-3352.
45. Helb, D., et al., *Rapid Detection of Mycobacterium tuberculosis and Rifampin Resistance by Use of On-Demand, Near-Patient Technology.* Journal of Clinical Microbiology, 2010. **48**(1): p. 229-237.

46. Banada, P.P., et al., *Containment of Bioaerosol Infection Risk by the Xpert MTB/RIF Assay and Its Applicability to Point-of-Care Settings.* Journal of Clinical Microbiology, 2010. **48**(10): p. 3551-3557.
47. Blakemore, R., et al., *Evaluation of the Analytical Performance of the Xpert MTB/RIF Assay.* Journal of Clinical Microbiology, 2010. **48**(7): p. 2495-2501.
48. Boehme, C.C., et al., *Rapid Molecular Detection of Tuberculosis and Rifampin Resistance.* New England Journal of Medicine, 2010. **363**(11): p. 1005-1015.
49. McNerney, R. and P. Daley, *Towards a point-of-care test for active tuberculosis: obstacles and opportunities.* Nature Reviews Microbiology, 2011. **9**(3): p. 204-213.
50. Bang, D., *The management of tuberculosis: epidemiology, resistance and monitoring Rapid methods to improve treatment outcome.* Danish Medical Bulletin, 2010. **57**(11).
51. Fennelly, K.P., et al., *Cough-generated aerosols of Mycobacterium tuberculosis - A new method to study infectiousness.* American Journal of Respiratory and Critical Care Medicine, 2004. **169**(5): p. 604-609.
52. Baussano, I., et al., *Tuberculosis among Health Care Workers.* Emerging Infectious Diseases, 2011. **17**(3): p. 488-494.
53. Bemer-Melchior, P., M.J. Gouzer'h, and H.B. Drugeon, *Laboratory transmission of Mycobacterium tuberculosis.* Infection Control and Hospital Epidemiology, 1998. **19**(8): p. 610-610.
54. Fatoyinbo, H.O., et al., *An integrated dielectrophoretic quartz crystal microbalance (DEP-QCM) device for rapid biosensing applications.* Biosensors & Bioelectronics, 2007. **23**(2): p. 225-232.
55. Gao, J., et al., *Hybrid electrokinetic manipulation in high-conductivity media.* Lab on a Chip, 2011. **11**(10): p. 1770-1775.
56. Wu, J., Y.X. Ben, and H.C. Chang, *Particle detection by electrical impedance spectroscopy with asymmetric-polarization AC electroosmotic trapping.* Microfluidics and Nanofluidics, 2005. **1**(2): p. 161-167.
57. Weigl, B., et al., *Towards non- and minimally instrumented, microfluidics-based diagnostic devices.* Lab on a Chip, 2008. **8**(12): p. 1999-2014.
58. Parsons, L.M., et al., *Laboratory diagnosis of tuberculosis in resource-poor countries: challenges and opportunities.* Clin Microbiol Rev, 2011. **24**(2): p. 314-50.

59. Fukushima, M., et al., *Detection and identification of Mycobacterium species isolates by DNA microarray.* J Clin Microbiol, 2003. **41**(6): p. 2605-15.
60. Clouse, K., et al., *Implementation of Xpert MTB/RIF for routine point-of-care diagnosis of tuberculosis at the primary care level.* S Afr Med J, 2012. **102**(10): p. 805-7.
61. Gaster, R.S., D.A. Hall, and S.X. Wang, *nanoLAB: an ultraportable, handheld diagnostic laboratory for global health.* Lab Chip, 2011. **11**(5): p. 950-6.
62. Chun, A.L., *Nanoparticles offer hope for TB detection.* Nat Nanotechnol, 2009. **4**(11): p. 698-9.
63. Kim, J.H., et al., *Immunosensor towards low-cost, rapid diagnosis of tuberculosis.* Lab on a Chip, 2012. **12**(8): p. 1437-1440.
64. Liu, J., et al., *Mycolic acid structure determines the fluidity of the mycobacterial cell wall.* Journal of Biological Chemistry, 1996. **271**(47): p. 29545-29551.
65. Horan, K.L., et al., *Isolation of the genome sequence strain Mycobacterium avium 104 from multiple patients over a 17-year period.* J Clin Microbiol, 2006. **44**(3): p. 783-9.
66. Yeo, W.H., et al., *Size-selective immunofluorescence of Mycobacterium tuberculosis cells by capillary- and viscous forces.* Lab on a Chip, 2010. **10**(22): p. 3178-3181.
67. Yeo, W.H., et al., *Size-Specific Concentration of DNA to a Nanostructured Tip Using Dielectrophoresis and Capillary Action.* Journal of Physical Chemistry B, 2009. **113**(31): p. 10849-10858.
68. Yeo, W.H., et al., *Rapid detection of Mycobacterium tuberculosis cells by using microtip-based immunoassay.* Analytical and Bioanalytical Chemistry, 2009. **393**(6-7): p. 1593-1600.
69. Kent, P.T. and G.P. Kubica, *Public Health Mycobacteriology*, in *A Guide for the Level III Laboratory* 1985, Centers for Disease Control and Prevention: Atlanta, GA.
70. Pfyffer, G.E., B.A. Brown-Elliot, and R.J. Wallace, *General characteristics, isolation and staining procedures*, in *Manual of Clinical Microbiology*. 2003, American Society for Microbiology Press: Washington, D. C. p. 532-559.
71. Smithwich, R.W., *Laboratory manual for acid-fast microscopy*. 1976, Centers for Disease Control: Atlanta, GA.

72. McClean, M., et al., *Identification and characterization of breakthrough contaminants associated with the conventional isolation of Mycobacterium tuberculosis.* Journal of Medical Microbiology, 2011. **60**(9): p. 1292-1298.
73. Zwadyk, P., et al., *Rendering of Mycobacteria Safe for Molecular Diagnostic Studies and Development of a Lysis Method for Strand Displacement Amplification and Pcr.* Journal of Clinical Microbiology, 1994. **32**(9): p. 2140-2146.
74. Hosek, J., et al., *Methods of mycobacterial DNA isolation from different biological material: a review.* Veterinarni Medicina, 2006. **51**(5): p. 180-192.
75. Liedtke, W., et al., *Different Methods of Sample Preparation Influence Sensitivity of Mycobacterium-Tuberculosis and Borrelia-Burgdorferi Pcr.* Pcr-Methods and Applications, 1994. **3**(5): p. 301-304.
76. Bemer-Melchior, P. and H.B. Drugeon, *Inactivation of Mycobacterium tuberculosis for DNA typing analysis.* Journal of Clinical Microbiology, 1999. **37**(7): p. 2350-2351.
77. Doig, C., et al., *The efficacy of the heat killing of Mycobacterium tuberculosis.* Journal of Clinical Pathology, 2002. **55**(10): p. 778-779.
78. LaBarre, P., et al., *A simple, inexpensive device for nucleic acid amplification without electricity-toward instrument-free molecular diagnostics in low-resource settings.* PLoS One, 2011. **6**(5): p. e19738.
79. Minion, J., et al., *Comparison of LED and conventional fluorescence microscopy for detection of acid fast bacilli in a low-incidence setting.* PLoS One, 2011. **6**(7): p. e22495.
80. Trusov, A., et al., *Comparison of Lumin LED fluorescent attachment, fluorescent microscopy and Ziehl-Neelsen for AFB diagnosis.* Int J Tuberc Lung Dis, 2009. **13**(7): p. 836-41.
81. Chung, C.C., et al., *Screening of Antibiotic Susceptibility to beta-Lactam-Induced Elongation of Gram-Negative Bacteria Based on Dielectrophoresis.* Analytical Chemistry, 2012. **84**(7): p. 3347-3354.
82. Hawkins, B.G., et al., *Automated Dielectrophoretic Characterization of Mycobacterium smegmatis.* Analytical Chemistry, 2011. **83**(9): p. 3507-3515.
83. Chung, C.C., et al., *Antibiotic susceptibility test based on the dielectrophoretic behavior of elongated Escherichia coli with cephalexin treatment.* Biomicrofluidics, 2011. **5**(2).

84. Whitesides, G.M., *The origins and the future of microfluidics.* Nature, 2006. **442**(7101): p. 368-73.
85. Cho, Y.K., et al., *Bacteria concentration using a membrane type insulator-based dielectrophoresis in a plastic chip.* Electrophoresis, 2009. **30**(18): p. 3153-3159.
86. Sanchis, A., et al., *Dielectric characterization of bacterial cells using dielectrophoresis.* Bioelectromagnetics, 2007. **28**(5): p. 393-401.
87. Das, C.M., et al., *Dielectrophoretic segregation of different human cell types on microscope slides.* Analytical Chemistry, 2005. **77**(9): p. 2708-2719.
88. Yang, J., et al., *Differential analysis of human leukocytes by dielectrophoretic field-flow-fractionation.* Biophysical Journal, 2000. **78**(5): p. 2680-2689.
89. Chou, C.F., et al., *Electrodeless dielectrophoresis of single- and double-stranded DNA.* Biophysical Journal, 2002. **83**(4): p. 2170-2179.
90. Holzel, R., *Dielectric and dielectrophoretic properties of DNA.* Iet Nanobiotechnology, 2009. **3**(2): p. 28-45.
91. Nakano, A. and A. Ros, *Protein dielectrophoresis: Advances, challenges, and applications.* Electrophoresis, 2013. **34**(7): p. 1085-1096.
92. Sasaki, N., T. Kitamori, and H.B. Kim, *AC electroosmotic micromixer for chemical processing in a microchannel.* Lab on a Chip, 2006. **6**(4): p. 550-554.
93. Huang, S.H., et al., *AC electroosmotic generated in-plane microvortices for stationary or continuous fluid mixing.* Sensors and Actuators B-Chemical, 2007. **125**(1): p. 326-336.
94. Studer, V., et al., *An integrated AC electrokinetic pump in a microfluidic loop for fast and tunable flow control.* Analyst, 2004. **129**(10): p. 944-9.
95. Debesset, S., et al., *An AC electroosmotic micropump for circular chromatographic applications.* Lab on a Chip, 2004. **4**(4): p. 396-400.
96. Mpholo, M., C.G. Smith, and A.B.D. Brown, *Low voltage plug flow pumping using anisotropic electrode arrays.* Sensors and Actuators B-Chemical, 2003. **92**(3): p. 262-268.
97. Grier, D.G., *A revolution in optical manipulation.* Nature, 2003. **424**(6950): p. 810-816.
98. Li, P., K.B. Shi, and Z.W. Liu, *Manipulation and spectroscopy of a single particle by use of white-light optical tweezers.* Optics Letters, 2005. **30**(2): p. 156-158.

99. Mirowski, E., et al., *Manipulation and sorting of magnetic particles by a magnetic force microscope on a microfluidic magnetic trap platform.* Applied Physics Letters, 2005. **86**(24).

100. Park, S., M. Koklu, and A. Beskok, *Particle Trapping in High-Conductivity Media with Electrothermally Enhanced Negative Dielectrophoresis.* Analytical Chemistry, 2009. **81**(6): p. 2303-2310.

101. Gielen, F., A.J. Demello, and J.B. Edel, *Dielectric Cell Response in Highly Conductive Buffers.* Analytical Chemistry, 2012. **84**(4): p. 1849-1853.

102. Lian, M., N. Islam, and J. Wu, *AC electrothermal manipulation of conductive fluids and particles for lab-chip applications.* Iet Nanobiotechnology, 2007. **1**(3): p. 36-43.

103. Park, S., et al., *Continuous dielectrophoretic bacterial separation and concentration from physiological media of high conductivity.* Lab on a Chip, 2011. **11**(17): p. 2893-2900.

104. Pohl, H.A., *DI ELECTROPHORESIS THE BEHAVIOR OF NEUTRAL MATTER IN NONUNIFORM ELECTRIC FIELDS*. Di Electrophoresis the Behavior of Neutral Matter in Nonuniform Electric Fields. 1978. 579.

105. Crane, J.S. and H.A. Pohl, *A Study of Living and Dead Yeast Cells Using Dielectrophoresis.* Journal of the Electrochemical Society, 1968. **115**(6): p. 584-&.

106. Castellarnau, M., et al., *Dielectrophoresis as a tool to characterize and differentiate isogenic mutants of Escherichia coli.* Biophysical Journal, 2006. **91**(10): p. 3937-3945.

107. Irimajiri, A., T. Hanai, and A. Inouye, *Dielectric Theory of Multi-Stratified Shell-Model with Its Application to a Lymphoma Cell.* Journal of Theoretical Biology, 1979. **78**(2): p. 251-269.

108. Huang, Y., et al., *Differences in the AC electrodynamics of viable and non-viable yeast cells determined through combined dielectrophoresis and electrorotation studies.* Phys Med Biol, 1992. **37**(7): p. 1499-517.

109. Zhao, H. and H.H. Bau, *Polarization of nanorods submerged in an electrolyte solution and subjected to an ac electrical field.* Langmuir, 2010. **26**(8): p. 5412-20.

110. Huang, J.P., et al., *Electrorotation in graded colloidal suspensions.* Physical Review E, 2003. **67**(5).

111. Huang, J.P., et al., *Spectral representation theory for dielectric behavior of nonspherical cell suspensions.* Communications in Theoretical Physics, 2002. **38**(1): p. 113-120.

112. Ramos, A., et al., *AC electric-field-induced fluid flow in microelectrodes.* Journal of Colloid and Interface Science, 1999. **217**(2): p. 420-422.
113. Ramos, A., et al., *Ac electrokinetics: a review of forces in microelectrode structures.* Journal of Physics D-Applied Physics, 1998. **31**(18): p. 2338-2353.
114. Schwan, H.P., *Electrode Polarization Impedance and Measurements in Biological Materials.* Annals of the New York Academy of Sciences, 1968. **148**(A1): p. 191-&.
115. Bard, A.J.a.F., L. R., *Electrochemical Methods, Funcamental and Applications*. 1980, New York: Wiley.
116. Green, N.G., et al., *Fluid flow induced by nonuniform ac electric fields in electrolytes on microelectrodes. III. Observation of streamlines and numerical simulation.* Physical Review E, 2002. **66**(2).
117. Oh, J., et al., *Comprehensive analysis of particle motion under non-uniform AC electric fields in a microchannel.* Lab on a Chip, 2009. **9**(1): p. 62-78.
118. Castellanos, A., et al., *Electrohydrodynamics and dielectrophoresis in microsystems: scaling laws.* Journal of Physics D-Applied Physics, 2003. **36**(20): p. 2584-2597.
119. Yeo, W.H., et al., *Nanotip analysis for dielectrophoretic concentration of nanosized viral particles.* Nanotechnology, 2013. **24**(18).
120. Kaprelyants, A.S. and D.B. Kell, *Rapid Assessment of Bacterial Viability and Vitality by Rhodamine 123 and Flow-Cytometry.* Journal of Applied Bacteriology, 1992. **72**(5): p. 410-422.
121. Suehiro, J., et al., *Selective detection of viable bacteria using dielectrophoretic impedance measurement method.* Journal of Electrostatics, 2003. **57**(2): p. 157-168.
122. Markx, G.H., M.S. Talary, and R. Pethig, *Separation of Viable and Nonviable Yeast Using Dielectrophoresis.* Journal of Biotechnology, 1994. **32**(1): p. 29-37.
123. Ratanachoo, K., P.R.C. Gascoyne, and M. Ruchirawat, *Detection of cellular responses to toxicants by dielectrophoresis.* Biochimica Et Biophysica Acta-Biomembranes, 2002. **1564**(2): p. 449-458.
124. Johari, J., et al., *Dielectrophoretic assay of bacterial resistance to antibiotics.* Physics in Medicine and Biology, 2003. **48**(14): p. N193-N198.

125. Pethig, R. and M.S. Talary, *Dielectrophoretic detection of membrane morphology changes in Jurkat T-cells undergoing etoposide-induced apoptosis.* Iet Nanobiotechnology, 2007. **1**(1): p. 2-9.
126. Patel, P. and G.H. Markx, *Dielectric measurement of cell death.* Enzyme and Microbial Technology, 2008. **43**(7): p. 463-470.
127. Pethig, R., *Dielectrophoresis: Using inhomogeneous AC electrical fields to separate and manipulate cells.* Critical Reviews in Biotechnology, 1996. **16**(4): p. 331-348.
128. Markx, G.H. and R. Pethig, *Dielectrophoretic Separation of Cells - Continuous Separation.* Biotechnology and Bioengineering, 1995. **45**(4): p. 337-343.
129. Hoffmann, C., et al., *Disclosure of the mycobacterial outer membrane: Cryo-electron tomography and vitreous sections reveal the lipid bilayer structure.* Proceedings of the National Academy of Sciences of the United States of America, 2008. **105**(10): p. 3963-3967.
130. Mitchison, D.A. and A.J. Nunn, *Influence of initial drug resistance on the response to short-course chemotherapy of pulmonary tuberculosis.* Am Rev Respir Dis, 1986. **133**(3): p. 423-30.
131. Somoskovi, A., L.M. Parsons, and M. Salfinger, *The molecular basis of resistance to isoniazid, rifampin, and pyrazinamide in Mycobacterium tuberculosis.* Respir Res, 2001. **2**(3): p. 164-8.
132. Felmlee, T.A., et al., *Genotypic detection of Mycobacterium tuberculosis rifampin resistance: comparison of single-strand conformation polymorphism and dideoxy fingerprinting.* J Clin Microbiol, 1995. **33**(6): p. 1617-23.
133. Telenti, A., et al., *Direct, automated detection of rifampin-resistant Mycobacterium tuberculosis by polymerase chain reaction and single-strand conformation polymorphism analysis.* Antimicrob Agents Chemother, 1993. **37**(10): p. 2054-8.
134. McClure, W.R. and C.L. Cech, *On the mechanism of rifampicin inhibition of RNA synthesis.* J Biol Chem, 1978. **253**(24): p. 8949-56.
135. Bardou, F., et al., *Mechanism of isoniazid uptake in Mycobacterium tuberculosis.* Microbiology, 1998. **144 (Pt 9)**: p. 2539-44.
136. Winder, F.G. and P.B. Collins, *Inhibition by isoniazid of synthesis of mycolic acids in Mycobacterium tuberculosis.* J Gen Microbiol, 1970. **63**(1): p. 41-8.

137. Takayama, K., L. Wang, and H.L. David, *Effect of isoniazid on the in vivo mycolic acid synthesis, cell growth, and viability of Mycobacterium tuberculosis.* Antimicrob Agents Chemother, 1972. **2**(1): p. 29-35.
138. Takayama, K., L. Wang, and R.S. Merkal, *Scanning electron microscopy of the H37Ra strain of Mycobacterium tuberculosis exposed to isoniazid.* Antimicrob Agents Chemother, 1973. **4**(1): p. 62-5.
139. Bardou, F., et al., *Effects of isoniazid on ultrastructure of Mycobacterium aurum and Mycobacterium tuberculosis and on production of secreted proteins.* Antimicrobial Agents and Chemotherapy, 1996. **40**(11): p. 2459-2467.
140. Vilcheze, C., et al., *Inactivation of the inhA-encoded fatty acid synthase II (FASII) enoyl-acyl carrier protein reductase induces accumulation of the FASI end products and cell lysis of Mycobacterium smegmatis.* Journal of Bacteriology, 2000. **182**(14): p. 4059-4067.
141. Brennan, P.J. and H. Nikaido, *The Envelope of Mycobacteria.* Annual Review of Biochemistry, 1995. **64**: p. 29-63.

VITA

Shinnosuke Inoue was born in Fukuoka, Japan on July 6th 1986. He started and finished his pursuit of higher education at University of Washington, starting with undergraduate studies in 2004, receiving his B.S. in mechanical engineering in 2009, and finally his doctorate in mechanical engineering in 2014. His interest lies in nanotechnology and biomedicine for the improvement of the human condition. He published in 4 peer-reviewed journals.